



A locking-free immersed finite element method for planar elasticity interface problems [☆]



Tao Lin ^{a,*}, Dongwoo Sheen ^b, Xu Zhang ^a

^a Department of Mathematics, Virginia Tech, Blacksburg, VA 24061, United States

^b Department of Mathematics, Seoul National University, Seoul 151-747, Republic of Korea

ARTICLE INFO

Article history:

Received 11 May 2012

Received in revised form 26 February 2013

Accepted 28 March 2013

Available online 10 April 2013

Keywords:

Elasticity interface problems
Nonconforming finite element
Immersed finite element
Cartesian mesh
Locking-free

ABSTRACT

This article proposes a nonconforming immersed finite element (IFE) method for solving planar elasticity interface problems with structured (or Cartesian) meshes even if the material interface has a nontrivial geometry. IFE functions developed in this article are applicable to arbitrary configurations of elasticity materials and interface locations. Optimal approximation capability is observed for this new IFE space. The displacement Galerkin method based on this IFE space is robust (locking-free). Numerical experiments are presented to demonstrate that the IFE solution converges optimally for both compressible and nearly incompressible materials.

© 2013 Elsevier Inc. All rights reserved.

1. Introduction

The partial differential equation (PDE) for linear elasticity plays an important role in solid mechanics. When used to model an object made of multiple elasticity materials separated by a definite interface, the coefficients in this partial differential equation are discontinuous, and are often piecewise constants. In addition to the usual boundary condition, the exact solution to this PDE also requires to satisfy the displacement and traction jump conditions across each material interface, and this leads to a so-called linear elasticity interface problem.

Solving elasticity interface problems appears in many physical and engineering applications. For instance, in minimum-compliance-design problems [1], one desires to find an optimal choice of stiffness tensor $E_{ijkl}(x, y)$ to minimize the compliance of a structure for increasing its stiffness. When an isotropic elastic body is considered, the stiffness tensor is a linear combination of Lamé parameters $\lambda(x, y)$ and $\mu(x, y)$ and this leads to an elasticity equilibrium equation, as seen in (1.1). In many cases, the design problems involve multiple material phases [2,3], and the Lamé parameters λ and μ of the joint elastic body are usually discontinuous across the material interfaces. Consequently, this leads to the linear elasticity interface problem. Other interesting applications include microstructural evolution [4,5], the atomic interactions [6], and problems in the crystalline materials [7], to name just a few.

In this article, we consider a planar object made of two elastic materials whose Lamé parameters are different, but the method presented here is readily extendable to an elasticity object with multiple materials. The model problem of interest is the following planar elasticity pure displacement problem:

[☆] This work is partially supported by NSF Grant 1016313, NRF 2011-0000344, and the Technology Innovation Program (100036459, Development of center to support QoLT industry and infrastructures) funded by the MKE/KEIT.

* Corresponding author. Tel.: +1 5402312766.

E-mail addresses: tlin@math.vt.edu (T. Lin), sheen@snu.ac.kr (D. Sheen), xuz@vt.edu (X. Zhang).

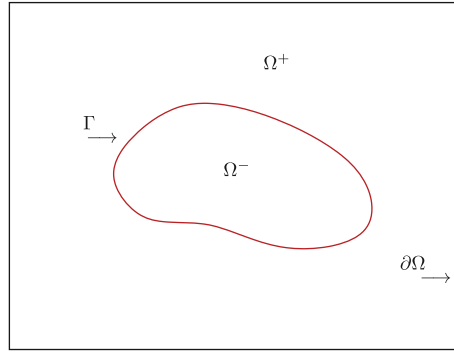


Fig. 1. The domain of elasticity interface problem.

$$-\nabla \cdot \boldsymbol{\sigma}(\mathbf{u}) = \mathbf{f} \text{ in } \Omega, \tag{1.1}$$

$$\mathbf{u} = \mathbf{g} \text{ on } \partial\Omega. \tag{1.2}$$

Without loss of generality, the solution domain $\Omega \subset \mathbb{R}^2$ is assumed to be a rectangle (or a union of several rectangles) formed with two types of elastic material separated by an interface Γ which is assumed to be a smooth curve. That means the domain Ω is the union of two disjoint sub-domains Ω^- and Ω^+ , each formed by one of the materials, such that $\Omega = \Omega^- \cup \Omega^+ \cup \Gamma$, as illustrated in Fig. 1. Across the interface Γ , the solution \mathbf{u} is assumed to satisfy the following jump conditions:

$$[\mathbf{u}]_\Gamma = \mathbf{0}, \tag{1.3}$$

$$[\boldsymbol{\sigma}(\mathbf{u}) \mathbf{n}]_\Gamma = \mathbf{0}. \tag{1.4}$$

In our discussion, we use letters in bold font to denote vector-valued functions and their associated function spaces. The function $\mathbf{u}(\mathbf{x}) = (u_1(x, y), u_2(x, y))^t$ denotes the displacement vector at a point $\mathbf{x} = (x, y)$ in the elastic body Ω . The vector \mathbf{n} denotes the outward normal of Γ . Function $\boldsymbol{\epsilon}(\mathbf{u}) = (\epsilon_{ij}(\mathbf{u}))_{1 \leq i, j \leq 2}$ denotes the linearized strain tensor defined by

$$\epsilon_{ij}(\mathbf{u}) = \frac{1}{2} \left(\frac{\partial u_i}{\partial x_j} + \frac{\partial u_j}{\partial x_i} \right)$$

and $\boldsymbol{\sigma}(\mathbf{u}) = (\sigma_{ij}(\mathbf{u}))_{1 \leq i, j \leq 2}$ is the stress tensor. Let λ and μ denote the Lamé parameters given by

$$\lambda = \frac{Ev}{(1 + \nu)(1 - 2\nu)}, \quad \mu = \frac{E}{2(1 + \nu)},$$

where E and ν are Young's modulus and Poisson's ratio, respectively, with $\nu \in (0, \frac{1}{2})$. Then, linear isotropic elastic materials are assumed to fulfill the following linear constitutive relation between the stress and strain tensors:

$$\sigma_{ij}(\mathbf{u}) = \lambda \text{Tr}(\boldsymbol{\epsilon}(\mathbf{u}))\delta_{ij} + 2\mu\epsilon_{ij}(\mathbf{u}),$$

where δ_{ij} denotes the Kronecker delta such that

$$\delta_{ij} = \begin{cases} 1 & \text{if } i = j, \\ 0 & \text{if } i \neq j \end{cases} \tag{1.5}$$

and $\text{Tr}(\boldsymbol{\epsilon})$ denotes the trace of tensor $\boldsymbol{\epsilon}$ so that

$$\text{Tr}(\boldsymbol{\epsilon}(\mathbf{u})) = \sum_{k=1}^2 \epsilon_{kk}(\mathbf{u}) = \nabla \cdot \mathbf{u}.$$

The function $\mathbf{f} = (f_1, f_2)^t$ represents the given body force and $\mathbf{g} = (g_1, g_2)^t$ is the given displacement on the boundary $\partial\Omega$. The Lamé parameters λ, μ are assumed to have a finite jump across the interface Γ such that

$$(\lambda(\mathbf{x}), \mu(\mathbf{x})) = \begin{cases} (\lambda^-, \mu^-), & \text{if } \mathbf{x} \in \Omega^-, \\ (\lambda^+, \mu^+), & \text{if } \mathbf{x} \in \Omega^+. \end{cases} \tag{1.6}$$

It is challenging to solve interface problems since the discontinuities across material interfaces require special care in numerical approximation. Conventional finite element methods [8–10] can work satisfactorily provided that meshes are tailored to fit interfaces, known as body-fitting meshes illustrated in the plot on the left in Fig. 2; otherwise, the convergence of numerical solutions is not guaranteed [11]. The body-fitting restriction makes conventional methods excessively expensive if interfaces evolve in a simulation. It is therefore attractive to develop numerical methods based on non-body-fitting meshes, such as the Cartesian mesh illustrated in the plot on the right in Fig. 2. In a finite difference formulation, Yang,

Li, and Li developed an immersed interface method for the planar linear elasticity interface problem which allows the interface to be embedded in the interior of some elements [12,13]. However, the linear systems arising from this method are non-symmetric and become ill-conditioned as the materials become nearly incompressible. In a finite element formulation, Hansbo and Hansbo developed a bilinear finite element method by employing a Nitsche's idea and a modified weak formulation using weighted average traction across the interfaces [14]. Becker, Burman, and Hansbo extended the Nitsche finite element method for incompressible elastic materials using a mixed formulation [15]. Hou, Li, Wang, and Wang [16] modified the traditional finite element method by designing a trial function that is a piecewise polynomial to fit jump condition across the interface while keeping the test function basis independent of interface. Due to the inconsistency of trial and test function spaces, the resulting linear system in this method is nonsymmetric, although positive-definiteness is guaranteed under certain conditions.

The recently developed immersed finite element (IFE) methods [17–26] locally adjust finite element basis functions to satisfy jump conditions across an interface. In IFE methods, solution meshes are allowed to be independent of interfaces; hence, if desired, a Cartesian mesh can be employed even if the interface geometry is nontrivial. Also IFE methods use standard finite element basis functions for all elements located away from interfaces, but they utilize IFE basis functions constructed according to jump conditions on elements whose interiors are cut by interfaces. In [18,24], Gong, Li, and Yang proposed linear IFE methods to solve elasticity interface problems on triangular Cartesian meshes. Point-wise convergence has been investigated, and numerical results indicate that the linear IFE solutions can achieve at least an $O(h)$ convergence in L^∞ norm. Recently, Lin and Zhang developed a bilinear IFE method [25] based on the rectangular Cartesian mesh. This article reported that both linear and bilinear IFE methods for the linear elasticity interface problem converge optimally in both L^2 and H^1 norms. Nevertheless, both of these IFE methods have limitations. First, the existence of these IFE functions is not guaranteed for arbitrary configuration of elastic materials in an interface problem [25]. Moreover, both of these IFE methods work well for compressible elastic materials, but once the elastic material is nearly incompressible, *i.e.*, Poisson's ratio $\nu \approx 0.5$, these IFE methods encounter the volume “locking” effect [27]. The “locking” effect arises when displacements are approximated by using the lowest-order conforming type finite elements even for solving non-interface problems. As we know, in either the linear or the bilinear IFE method, the majority of elements do not intersect the material interface, where standard conforming type finite element functions are utilized; hence, the “locking” can be considered inevitable for these IFE methods.

Several approaches have been developed to circumvent the ‘locking’ effect, such as the mixed finite element methods [28–34], the nonconforming finite element methods [30,35,32,36–39], and the discontinuous Galerkin methods [40–43]. In this article, we follow the route of nonconforming finite elements due to its simple formulation compared with other ideas. We construct new IFE functions that are consistent with nonconforming rotated- Q_1 (abbreviated as $\mathcal{NCR}Q_1$, from now on) finite element functions on a rectangular mesh in the sense that an IFE function becomes a $\mathcal{NCR}Q_1$ finite element function if the discontinuity of the Lamé coefficients disappears. The $\mathcal{NCR}Q_1$ element was first proposed in [44] for solving the Stokes problem. It was also used for linear elasticity problems [37]. Instead of using nodal values as continuity constraints in the conforming finite element formulation, the $\mathcal{NCR}Q_1$ finite element uses averaged values over edges as constraints. As indicated in [37], the method using the $\mathcal{NCR}Q_1$ finite element on a mesh made of quadrilateral elements does not have numerical locking provided that a reduced quadrature procedure is applied to treat the integral containing the λ term, *i.e.* $\int_T \lambda (\nabla \cdot \mathbf{u}_h) (\nabla \cdot \mathbf{v}_h) dx dy$. This reduced integration technique has been used widely in engineering community and analyzed by mathematicians [45,35,31,46–48,33]. On the other hand, though it still needs to be proven theoretically, our numerical experiments indicate that the reduced integration is not necessary to circumvent numerical locking if the $\mathcal{NCR}Q_1$ element is used on a rectangular mesh.

The rest of the article is organized as follows. In Section 2, we introduce an $\mathcal{NCR}Q_1$ -IFE space based on a rectangular mesh. In Section 3, we discuss basic properties of this new IFE space. In Section 4, we apply this IFE space in a Galerkin formulation to solve the planar elasticity interface problems. In Section 5, we provide numerical results to demonstrate features of this nonconforming IFE method, including its optimal approximation capability and its “locking free” performance for linear elasticity interface problems with nearly incompressible materials. Brief conclusions are given in Section 6.

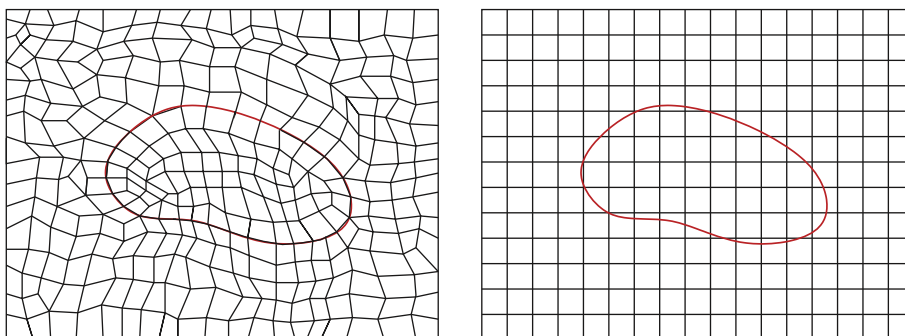


Fig. 2. Body-fitting mesh and non-body-fitting mesh.

2. Nonconforming rotated Q_1 IFE spaces

In this section, we introduce the $\mathcal{NCR}Q_1$ -IFE functions and corresponding IFE spaces defined on a rectangular mesh.

For $0 < h < 1$, let $\mathcal{T}_h = \{T_j, j = 1, \dots, M\}$ be a Cartesian mesh of Ω with maximum edge length h . We call the elements whose interiors are cut through by Γ “interface elements”, and denote the set of interface elements by \mathcal{T}_h^i . We use $\mathcal{T}_h^n = \mathcal{T}_h \setminus \mathcal{T}_h^i$ to denote the collection of non-interface elements. Moreover, we let \mathcal{E}_h represent the collection of all the edges in \mathcal{T}_h , and denote the collections of interior edges and boundary edges by \mathcal{E}_h^o and \mathcal{E}_h^b , respectively.

2.1. $\mathcal{NCR}Q_1$ -IFE functions on non-interface elements

Standard $\mathcal{NCR}Q_1$ finite element functions will be used on non-interface elements: for $T \in \mathcal{T}_h^n$, define the local finite element space $\mathbf{S}_h^n(T)$ as follows:

$$\mathbf{S}_h^n(T) = \{ \Psi_T = (\psi_{1,T}, \psi_{2,T})^t : \psi_{j,T} \in \mathcal{NCR}Q_1, \quad j = 1, 2 \}, \tag{2.1}$$

where $\mathcal{NCR}Q_1 = \text{Span}\{1, x, y, x^2 - y^2\}$. Eight local basis functions $\Psi_{j,T} \in \mathbf{S}_h^n(T)$, $j = 1, \dots, 8$, are chosen to satisfy the following edge average value restrictions:

$$\frac{1}{|e_k|} \int_{e_k} \Psi_{j,T}(x, y) \, ds = \begin{pmatrix} \delta_{jk} \\ 0 \end{pmatrix}, \quad j = 1, 2, 3, 4 \tag{2.2}$$

and

$$\frac{1}{|e_k|} \int_{e_k} \Psi_{j,T}(x, y) \, ds = \begin{pmatrix} 0 \\ \delta_{j-4,k} \end{pmatrix}, \quad j = 5, 6, 7, 8, \tag{2.3}$$

where $e_k, k = 1, 2, 3, 4$ are four edges of T . We refer readers to [37,44,49] and references therein for more details about the standard $\mathcal{NCR}Q_1$ finite element functions.

2.2. $\mathcal{NCR}Q_1$ -IFE functions on interface elements

Without loss of generality, we assume that the mesh size h is small enough such that interface elements in \mathcal{T}_h satisfy the following hypotheses [19,20,25]:

- (H1) The interface Γ cannot intersect the edge of any rectangular element at more than two points unless an edge of the boundary is part of Γ ;
- (H2) If Γ intersects the edge of a rectangular element at two points, then these two points must be on different edges of this rectangular element.

Assume that T is an interface element whose boundary intersects Γ at points D and E . First, we note that there are two types of interface elements: if D and E are located at two adjacent edges, we classify this element as Type I interface element; if D and E are located at two opposite edges, we classify this element as Type II interface element. Fig. 3 provides illustrations for these two types of interface elements. The line \overline{DE} separates T into two sub-elements T^- and T^+ .

Without loss of generality, we consider a typical interface element $T = \square A_1 A_2 A_3 A_4$ with vertices

$$A_1 = \begin{pmatrix} 0 \\ 0 \end{pmatrix}, \quad A_2 = \begin{pmatrix} h \\ 0 \end{pmatrix}, \quad A_3 = \begin{pmatrix} 0 \\ h \end{pmatrix}, \quad A_4 = \begin{pmatrix} h \\ h \end{pmatrix}.$$

We label the four edges $e_i, i = 1, 2, 3, 4$, of T as follows:

$$e_1 = \overline{A_1 A_2}, \quad e_2 = \overline{A_2 A_4}, \quad e_3 = \overline{A_4 A_3}, \quad e_4 = \overline{A_3 A_1}. \tag{2.4}$$

We also assume that

$$D = \begin{pmatrix} dh \\ 0 \end{pmatrix}, \quad E = \begin{pmatrix} 0 \\ eh \end{pmatrix}$$

for a Type I interface element, where $0 < d \leq 1, 0 < e \leq 1$, and

$$D = \begin{pmatrix} dh \\ 0 \end{pmatrix}, \quad E = \begin{pmatrix} eh \\ h \end{pmatrix}$$

for a Type II interface element, where $0 < d < 1$ and $0 < e < 1$. We note that every interface element can be mapped into one of the above interface elements via an orthogonal affine mapping.

Vector-valued piecewise $\mathcal{NCR}Q_1$ polynomials are used to construct nonconforming local IFE functions on each interface element. Specifically, on an interface element T , a local $\mathcal{NCR}Q_1$ -IFE function Φ_T is piecewisely defined as follows:

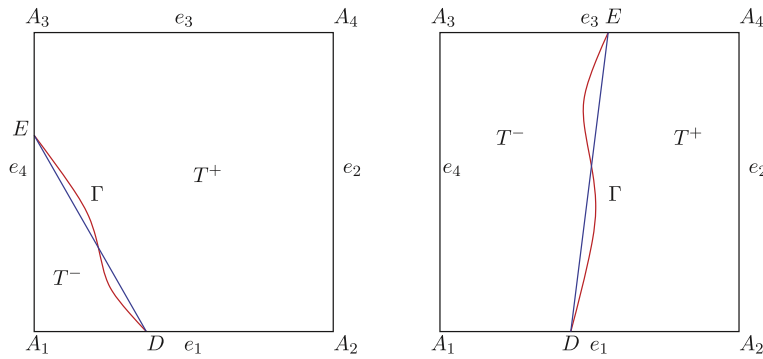


Fig. 3. Types of interface nonconforming rectangles.

$$\Phi_T(\mathbf{x}) = \begin{cases} \Phi_T^-(\mathbf{x}) = \begin{pmatrix} \phi_{1,T}^-(x,y) \\ \phi_{2,T}^-(x,y) \end{pmatrix} = \begin{pmatrix} a_1^- + b_1^-x + c_1^-y + d_1^-(x^2 - y^2) \\ a_2^- + b_2^-x + c_2^-y + d_2^-(x^2 - y^2) \end{pmatrix} & \text{if } \mathbf{x} \in T^-, \\ \Phi_T^+(\mathbf{x}) = \begin{pmatrix} \phi_{1,T}^+(x,y) \\ \phi_{2,T}^+(x,y) \end{pmatrix} = \begin{pmatrix} a_1^+ + b_1^+x + c_1^+y + d_1^+(x^2 - y^2) \\ a_2^+ + b_2^+x + c_2^+y + d_2^+(x^2 - y^2) \end{pmatrix} & \text{if } \mathbf{x} \in T^+. \end{cases} \quad (2.5)$$

Note that for each Φ_T defined above, there are 16 undetermined coefficients, $a_j^s, b_j^s, c_j^s, d_j^s$, where $j = 1, 2$, and $s = +, -$. For eight given values $v_j, j = 1, \dots, 8$, the following constraints will be used to determine these coefficients:

- the average values over the edges (8 restrictions):

$$\frac{1}{|e_j|} \int_{e_j} \Phi_T(x,y) ds = \begin{pmatrix} v_j \\ v_{j+4} \end{pmatrix}, \quad \forall j = 1, 2, 3, 4. \quad (2.6)$$

- the displacement continuity at the intersection points (4 restrictions):

$$\Phi_T^+(D) = \Phi_T^-(D), \quad \Phi_T^+(E) = \Phi_T^-(E). \quad (2.7)$$

- the weak traction continuity (2 restrictions):

$$\int_{\overline{DE}} \sigma(\Phi_T^+) \mathbf{n}_{\overline{DE}} ds = \int_{\overline{DE}} \sigma(\Phi_T^-) \mathbf{n}_{\overline{DE}} ds. \quad (2.8)$$

- the second derivative continuity (2 restrictions):

$$\frac{\partial^2 \Phi_T^+}{\partial x^2} = \frac{\partial^2 \Phi_T^-}{\partial x^2}. \quad (2.9)$$

We will show that these conditions are linearly independent so that they can uniquely determine a local \mathcal{NCR}_{Q_1} IFE function Φ_T on an interface element T . Note that, to maintain the continuity across \overline{DE} , instead of (2.9), it seems to be more natural to impose the following condition:

$$\Phi_T^+\left(\frac{D+E}{2}\right) = \Phi_T^-\left(\frac{D+E}{2}\right), \quad (2.10)$$

because $[\Phi_T]_{\overline{DE}}$ is a quadratic polynomial which can usually be determined by its values at three points. However, when the slope of \overline{DE} is 1 or -1 , conditions (2.7) and (2.10) lose their linear independence. On the other hand, (2.7) and (2.9) are always linearly independent. In addition, when the slope of \overline{DE} is not 1 or -1 , conditions (2.7) and (2.9) are equivalent to (2.7) and (2.10). These observations suggest us to use (2.9) instead of (2.10).

Remark 2.1. The condition (2.8) ensures that the IFE function Φ_T can weakly (in the sense of integration) preserve the traction continuity across the line segment \overline{DE} .

The combination of conditions in (2.6)–(2.9) provides 16 constraints for a local \mathcal{NCR}_{Q_1} -IFE function, and this leads to the following algebraic system to determine $a_j^s, b_j^s, c_j^s, d_j^s, j = 1, 2, s = +, -$:

$$M_C \mathbf{C} = \mathbf{V}, \quad (2.11)$$

where

$$\mathbf{C} = (a_1^-, a_1^+, a_2^-, a_2^+, b_1^-, b_1^+, b_2^-, b_2^+, c_1^-, c_1^+, c_2^-, c_2^+, d_1^-, d_1^+, d_2^-, d_2^+)^t,$$

where the components denoted by * are specified as follows:

$$\begin{aligned}
 m_{15,5}^{\parallel} &= \lambda^- + 2\mu^-, & m_{15,6}^{\parallel} &= -(\lambda^+ + 2\mu^+), & m_{15,7}^{\parallel} &= d\mu^- - e\mu^-, \\
 m_{15,8}^{\parallel} &= -d\mu^+ + e\mu^+, & m_{15,9}^{\parallel} &= d\mu^- - e\mu^-, & m_{15,10}^{\parallel} &= -d\mu^+ + e\mu^+, \\
 m_{15,11}^{\parallel} &= \lambda^-, & m_{15,12}^{\parallel} &= -\lambda^+, & m_{15,13}^{\parallel} &= (d+e)\lambda^- + (d+3e)\mu^-, \\
 m_{15,14}^{\parallel} &= -(d+e)\lambda^+ - (d+3e)\mu^+, & m_{15,15}^{\parallel} &= \lambda^- + (d^2 - e^2)\mu^-, & m_{15,16}^{\parallel} &= \lambda^+ - (d^2 - e^2)\mu^+, \\
 m_{16,5}^{\parallel} &= (d-e)\lambda^-, & m_{16,6}^{\parallel} &= -(d-e)\lambda^+, & m_{16,7}^{\parallel} &= \mu^-, \\
 m_{16,8}^{\parallel} &= -\mu^+, & m_{16,9}^{\parallel} &= \mu^-, & m_{16,10}^{\parallel} &= -\mu^+, \\
 m_{16,11}^{\parallel} &= (d-e)(\lambda^- + 2\mu^-), & m_{16,12}^{\parallel} &= -(d-e)\lambda^+ - (2d-2e)\mu^+, & m_{16,13}^{\parallel} &= (d^2 - e^2)\lambda^- \mu^-, \\
 m_{16,14}^{\parallel} &= -(d^2 - e^2)\lambda^+ + \mu^+, & m_{16,15}^{\parallel} &= -(d-e)\lambda^- - (d-3e)\mu^-, & m_{16,16}^{\parallel} &= (d-e)\lambda^+ + (d-3e)\mu^+.
 \end{aligned}$$

For each $j = 1, \dots, 8$, let $\mathbf{V}_j \in \mathbb{R}^{16}$ denote the j -th standard unit vector of form in (2.12). Then for $j = 1, \dots, 8$, with $\mathbf{V} = \mathbf{V}_j$ in (2.11), we can solve for $\mathbf{C} = \mathbf{C}_j$ and use it in (2.5) to form the j -th \mathcal{NCRQ}_1 -IFE local basis function $\Phi_{j,T}$, for either Type I or Type II interface element.

A typical \mathcal{NCRQ}_1 local basis function $\Psi_{4,T}$ on a non-interface element is illustrated in Fig. 4. As a comparison, the local \mathcal{NCRQ}_1 -IFE basis functions $\Phi_{4,T}$ on Type I and Type II interface elements are illustrated in Figs. 5 and 6, respectively. Note that, while the second component of $\Psi_{4,T}$ is zero, the second component of $\Phi_{4,T}$ is not completely zero because $\Phi_{4,T}$ is constructed to satisfy the interface jump conditions (2.6)–(2.9).

On each interface element T , the local \mathcal{NCRQ}_1 -IFE space $\mathbf{S}_h^i(T)$ is then given by

$$\mathbf{S}_h^i(T) = \text{Span}\{\Phi_{j,T} : j = 1, \dots, 8\}. \tag{2.15}$$

Then, the global \mathcal{NCRQ}_1 -IFE space is defined accordingly as

$$\mathbf{S}_h(\Omega) = \left\{ \Phi \in (L^2(\Omega))^2 : \Phi|_T \in \mathbf{S}_h^i(T) \text{ for } T \in \mathcal{T}_h^\alpha, \alpha = i, n, \forall T \in \mathcal{T}_h : \int_{\partial T_j \cap \partial T_k} \Phi|_{T_j} ds = \int_{\partial T_j \cap \partial T_k} \Phi|_{T_k} ds, \forall j, k \right\}. \tag{2.16}$$

3. Properties of nonconforming rotated Q_1 IFE spaces

In this section, we discuss basic properties of \mathcal{NCRQ}_1 -IFE basis functions and the corresponding IFE spaces.

3.1. Basic properties

Lemma 3.1 (Continuity). $\forall T \in \mathcal{T}_h^i, \mathbf{S}_h^i(T) \subset \mathbf{C}(T)$.

Proof. Note that every function $\Phi_T \in \mathbf{S}_h^i(T)$ is a piecewise polynomial; hence, it suffices to show Φ_T is continuous across the line segment \overline{DE} . The jump function $[\Phi_T]$ is linear since Φ_T satisfies the condition (2.9). Then, $[\Phi_T] = \mathbf{0}$ follows from (2.7).

Lemma 3.2 (Partition of unity). $\forall T \in \mathcal{T}_h^i$, the \mathcal{NCRQ}_1 -IFE local basis functions $\Phi_{j,T} \in \mathbf{S}_h^i(T), j = 1, \dots, 8$, fulfill

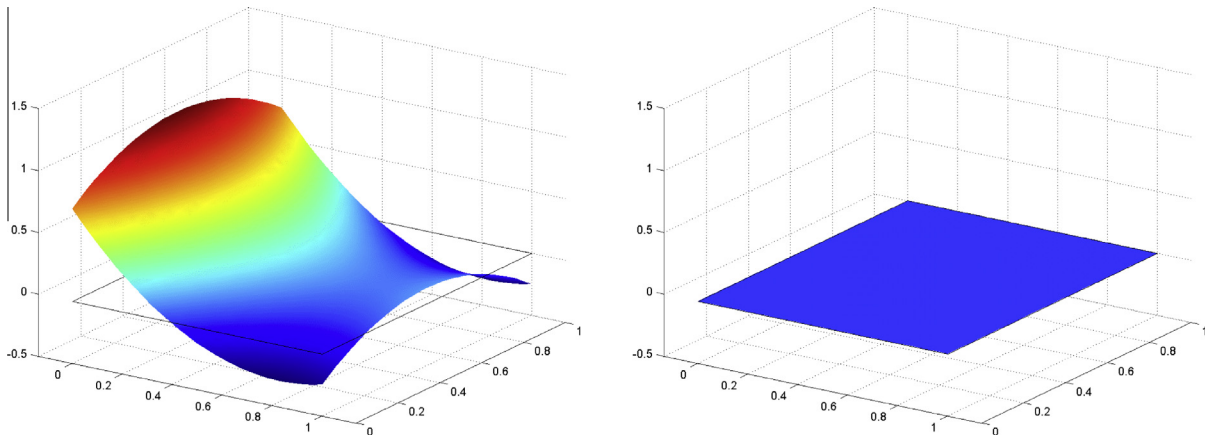


Fig. 4. The standard \mathcal{NCRQ}_1 FE local basis function $\Psi_{4,T}$: the left plot is for the first component $\psi_{4,T}$, and the right one is for the second component 0.

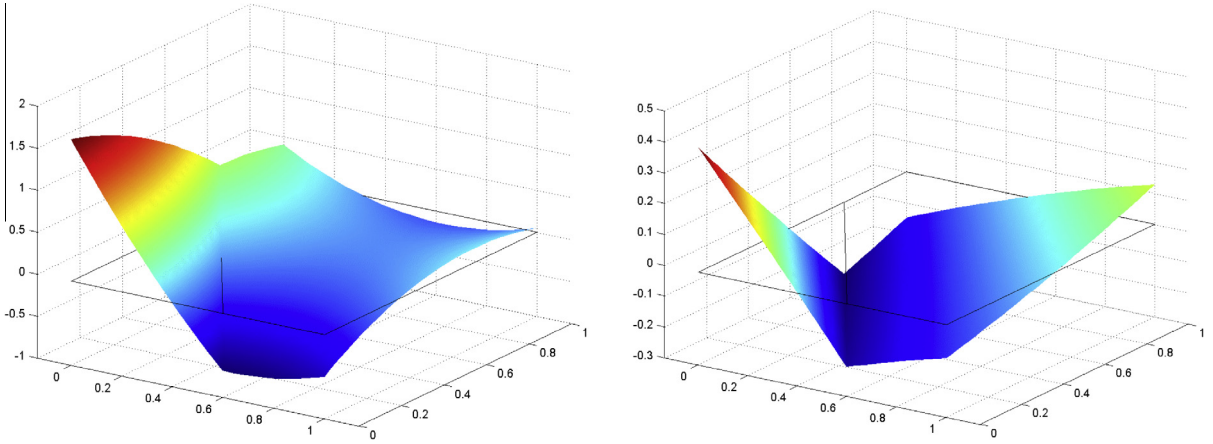


Fig. 5. The \mathcal{NCRQ}_1 -IFE basis functions $\Phi_{4,T}$ on the Type I interface element: the left plot is for the first component of $\Phi_{4,T}$, and the right plot is for its second component with $\lambda^+ = 20, \lambda^- = 1, \mu^+ = 2, \mu^- = 1, D = (0.6, 0)^t, E = (0, 0.7)^t$.

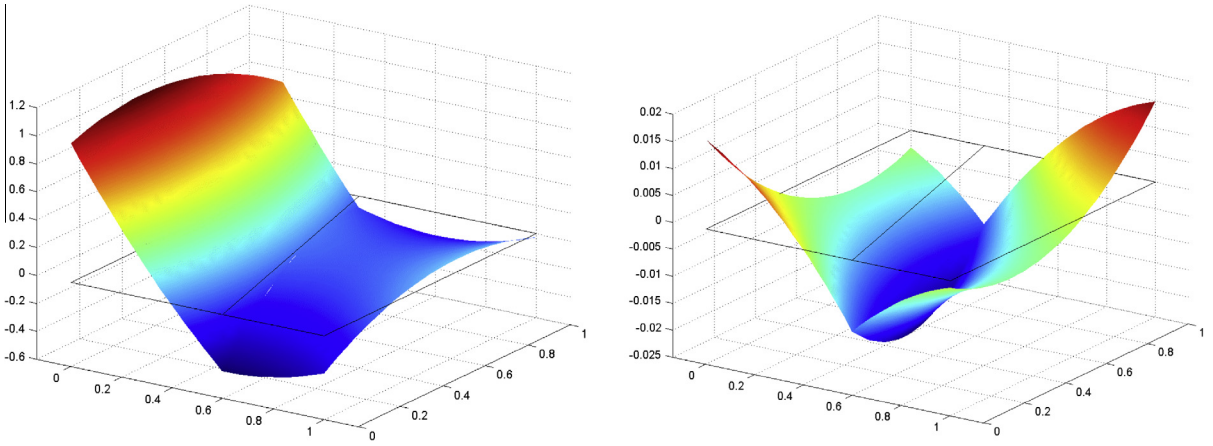


Fig. 6. The \mathcal{NCRQ}_1 -IFE basis functions $\Phi_{4,T}$ on the Type II interface element: the left plot is for the first component of $\Phi_{4,T}$, and the right plot is for its second component with $\lambda^+ = 20, \lambda^- = 1, \mu^+ = 2, \mu^- = 1, D = (0.6, 0)^t, E = (0.3, 1)^t$.

$$\sum_{j=1}^4 \Phi_{j,T}(x,y) = \begin{pmatrix} 1 \\ 0 \end{pmatrix}, \text{ and } \sum_{j=5}^8 \Phi_{j,T}(x,y) = \begin{pmatrix} 0 \\ 1 \end{pmatrix}. \tag{3.1}$$

Proof. By direct calculations, we obtain the following

$$\sum_{j=1}^4 a_{j,1}^- = 1, \quad \sum_{j=1}^4 b_{j,1}^- = 0, \quad \sum_{j=1}^4 c_{j,1}^- = 0, \quad \sum_{j=1}^4 d_{j,1}^- = 0.$$

$$\sum_{j=1}^4 a_{j,2}^- = 1, \quad \sum_{j=1}^4 b_{j,2}^- = 0, \quad \sum_{j=1}^4 c_{j,2}^- = 0, \quad \sum_{j=1}^4 d_{j,2}^- = 0.$$

$$\sum_{j=1}^4 a_{j,1}^+ = 1, \quad \sum_{j=1}^4 b_{j,1}^+ = 0, \quad \sum_{j=1}^4 c_{j,1}^+ = 0, \quad \sum_{j=1}^4 d_{j,1}^+ = 0.$$

$$\sum_{j=1}^4 a_{j,2}^+ = 1, \quad \sum_{j=1}^4 b_{j,2}^+ = 0, \quad \sum_{j=1}^4 c_{j,2}^+ = 0, \quad \sum_{j=1}^4 d_{j,2}^+ = 0.$$

This proves the first equation in (3.1). A similar argument can be carried out to show the second equation. \square

The following lemma indicates that the $\mathcal{NCR}Q_1$ -IFE basis functions are consistent with standard $\mathcal{NCR}Q_1$ finite element basis functions.

Lemma 3.3 (Consistency). $\forall T \in \mathcal{T}_h^i$, the $\mathcal{NCR}Q_1$ -IFE local basis functions $\Phi_{j,T} \in \mathbf{S}_h^i(T), j = 1, \dots, 8$, and the standard $\mathcal{NCR}Q_1$ -FE basis functions $\Psi_{j,T}, j = 1, \dots, 8$, are identical, i.e., $\Phi_{j,T} = \Psi_{j,T}, j = 1, \dots, 8$, under each of the following conditions:

- the elasticity parameters have no discontinuity, i.e., $\lambda^+ = \lambda^-, \mu^+ = \mu^-$;
- $\min\{|T^-|, |T^+|\}$ shrinks to zero, where $|T^s|, s = -, +$, denotes the area of the polygon T^s .

Proof. Consider the first case. Let $\lambda^+ = \lambda^-$ and $\mu^+ = \mu^-$ and solve the system (2.11). A direct calculation results in $\Phi_{j,T} = \Psi_{j,T}, j = 1, \dots, 8$.

Consider the second case. Without loss of generality, we assume $|T^-| \rightarrow 0$. Then for Type I interface element, we have either $d \rightarrow 0$, or $e \rightarrow 0$; for Type II interface element, we have both $d \rightarrow 0$ and $e \rightarrow 0$. A direct calculation shows that $\Phi_{j,T}^+ \rightarrow \Psi_{j,T}, j = 1, \dots, 8$ for both interface element Types. Also note that under this assumption, $\Phi_{j,T}$ becomes $\Phi_{j,T}^+$. \square

3.2. Unisolvency properties

We now consider the important unisolvency property: an IFE function is uniquely determined by constraints given either at the nodes or edges together with suitably designed interface jump conditions. Note that all scalar IFE functions developed for solving second order elliptic interface problems have the unisolvency property [50,21,23,51]. But for the planar elasticity interface problem, both linear [18,24] and bilinear [25] IFE functions have the unisolvency property conditionally. In fact, a counter-example was presented in [25] to show that there exist no linear IFE functions for a certain configuration of the interface and the Lamé parameters. This limitation of linear and bilinear IFE functions for the planar elasticity interface problem hinders their applications. Therefore it is critical to know whether the nonconforming rotated Q_1 IFE functions also suffer from this shortcoming. Fortunately, the answer is no.

For the Type I interface element, the determinant of matrix M_C^I can be written as follows

$$\det(M_C^I) = P_1^I \lambda^+ \mu^+ + P_2^I \lambda^- \mu^+ + P_3^I \mu^+ \mu^+ + P_4^I \lambda^+ \mu^- + P_5^I \lambda^- \mu^- + P_6^I \mu^+ \mu^- + P_7^I \mu^- \mu^-, \tag{3.2}$$

where

$$\begin{aligned} P_1^I &= d^2 e^2 (8d^2 - 3d^3 - 6de + 3d^2 e + 2e^2 - 3de^2 + 3e^3) (2d^2 + 3d^3 - 6de - 3d^2 e + 8e^2 + 3de^2 - 3e^3), \\ P_2^I &= de (9d^7 e + 20e^4 - 18d^6 e (1 + e) + d^5 e (-16 + 18e + 27e^2) + 4d^4 (5 + 15e^2 - 9e^4) + 2d^2 e^2 (20 + 30e^2 + 9e^3 - 9e^4) \\ &\quad + de^3 (-24 - 16e^2 - 18e^3 + 9e^4) + d^3 e (-24 - 104e^2 + 27e^4)), \\ P_3^I &= 2d^2 e^2 (5d^2 - 6de + 5e^2)^2, \\ P_4^I &= P_2^I, P_5^I = (4d^2 - 8d^3 e + 3d^4 e + 4e^2 + 6d^2 e^2 - 3d^3 e^2 - 2de^3 + 3d^2 e^3 - 3de^4) \\ &\quad (4d^2 - 2d^3 e - 3d^4 e + 4e^2 + 6d^2 e^2 + 3d^3 e^2 - 8de^3 - 3d^2 e^3 + 3de^4), \\ P_6^I &= 4de (5d^2 - 6de + 5e^2) (4d^2 - 5d^3 e + 4e^2 + 6d^2 e^2 - 5de^3), \\ P_7^I &= 2(-4d^2 + 5d^3 e - 4e^2 - 6d^2 e^2 + 5de^3)^2. \end{aligned}$$

Lemma 3.4. Assume that $0 < d \leq 1$ and $0 < e \leq 1$. Then we have

$$P_j^I > 0, \text{ for } j = 1, \dots, 7. \tag{3.3}$$

Proof. We can verify (3.3) by direct computations. For instance,

$$\begin{aligned} P_1^I &= d^2 e^2 \left(\frac{1}{2} (3d - 2e)^2 + 3d^2 (1 - d) + \frac{1}{2} d^2 + \frac{3}{2} e (d^2 + e^2) + \frac{3}{2} e (d - e)^2 \right) \\ &\quad \left(\frac{1}{2} (3e - 2d)^2 + 3e^2 (1 - e) + \frac{1}{2} e^2 + \frac{3}{2} d (d^2 + e^2) + \frac{3}{2} d (d - e)^2 \right) \geq \frac{d^4 e^4}{4}. \end{aligned}$$

Similar arguments apply to $P_j^I, j = 2, 3, \dots, 7$. \square

For Type II interface element, we note from (2.14) that,

$$\det(M_C^{II}) = P_1^{II} \lambda^+ \mu^+ + P_2^{II} \lambda^- \mu^+ + P_3^{II} \mu^+ \mu^+ + P_4^{II} \lambda^+ \mu^- + P_5^{II} \lambda^- \mu^- + P_6^{II} \mu^+ \mu^- + P_7^{II} \mu^- \mu^-, \tag{3.4}$$

where

$$\begin{aligned}
 P_1^II &= (5d - 9d^2 + 11d^3 - 3d^4 + 5e - 6de + d^2e - 3e^2 + de^2 - e^3 + 3e^4) \\
 &\quad (5d - 3d^2 - d^3 + 3d^4 + 5e - 6de + d^2e - 9e^2 + de^2 + 11e^3 - 3e^4), \\
 P_2^II &= 20d - 49d^2 + 100d^3 - 101d^4 + 44d^5 + 29d^6 - 36d^7 + 9d^8 + 20e - 74de + 104d^2e - 108d^3e \\
 &\quad + 36d^4e - 10d^5e - 49e^2 + 104de^2 - 146d^2e^2 + 136d^3e^2 - 29d^4e^2 + 100e^3 - 108de^3 \\
 &\quad + 136d^2e^3 - 124d^3e^3 + 36d^4e^3 - 101e^4 + 36de^4 - 29d^2e^4 + 36d^3e^4 - 18d^4e^4 + 44e^5 - 10de^5 + 29e^6 - 36e^7 + 9e^8, \\
 P_3^II &= 2(5d - 6d^2 + 5d^3 + 5e - 6de + d^2e - 6e^2 + de^2 + 5e^3)^2, \\
 P_4^II &= P_2^II, \\
 P_5^II &= (4 - 5d + 13d^2 - 11d^3 + 3d^4 - 5e - 2de - d^2e + 7e^2 - de^2 + e^3 - 3e^4) \\
 &\quad (4 - 5d + 7d^2 + d^3 - 3d^4 - 5e - 2de - d^2e + 13e^2 - de^2 - 11e^3 + 3e^4), \\
 P_6^II &= 4(4 - 5d + 10d^2 - 5d^3 - 5e - 2de - d^2e + 10e^2 - de^2 - 5e^3) \\
 &\quad (5d - 6d^2 + 5d^3 + 5e - 6de + d^2e - 6e^2 + de^2 + 5e^3), \\
 P_7^II &= 2(-4 + 5d - 10d^2 + 5d^3 + 5e + 2de + d^2e - 10e^2 + de^2 + 5e^3)^2.
 \end{aligned}$$

Similarly, we can show the following lemma.

Lemma 3.5. Assume that $0 < d < 1$ and $0 < e < 1$. Then we get

$$P_j^II > 0, \text{ for } j = 1, \dots, 7. \tag{3.5}$$

A combination of Lemmas 3.4 and 3.5 implies that the matrix M_C is nonsingular for both Type I and Type II interface elements. Consequently, we conclude that the \mathcal{NCR}_{Q_1} -IFE functions developed in the previous section do have the unisolvency property.

Theorem 3.1. The \mathcal{NCR}_{Q_1} -IFE functions defined by (2.5) for the planar elasticity interface problem are uniquely determined by the average values over edges of T as given in (2.6).

Remark 3.1. In contrast to the conditional unisolvency property of linear and bilinear IFE functions [25], Theorem 3.1 guarantees the availability of \mathcal{NCR}_{Q_1} -IFE functions for any configuration of elasticity materials and interface location. This is a significant advantage of our new IFE basis functions over those previously developed.

4. Interpolation and displacement Galerkin method

4.1. \mathcal{NCR}_{Q_1} -IFE interpolation

To investigate the approximation capability of these new IFE spaces, we consider the IFE interpolation defined as follows. In contrast to the conventional Lagrange type interpolation, the interpolation with \mathcal{NCR}_{Q_1} -IFE basis functions uses average values over element edges for the given function.

Assuming that \mathcal{T}_h is a Cartesian mesh of Ω , we define the local interpolation operator $\mathbf{I}_{h,T} : \mathbf{H}^1(T) \rightarrow \mathbf{S}_h(T)$ by

$$\mathbf{I}_{h,T}(\mathbf{u}) = \begin{cases} \sum_{j=1}^8 c_j \Phi_{j,T} & \text{if } T \in \mathcal{T}_h^i, \\ \sum_{j=1}^8 c_j \Psi_{j,T} & \text{if } T \in \mathcal{T}_h^n, \end{cases} \tag{4.1}$$

where

$$\begin{pmatrix} c_j \\ c_{j+4} \end{pmatrix} = \frac{1}{|e_j|} \int_{e_j} \mathbf{u}(x, y) \, ds, \quad j = 1, 2, 3, 4. \quad (4.2)$$

The global IFE interpolation operator $\mathbf{I}_h : \mathbf{H}^1(\Omega) \rightarrow \mathbf{S}_h(\Omega)$ is defined element by element as follows:

$$(\mathbf{I}_h \mathbf{u})|_T = \mathbf{I}_{h,T}(\mathbf{u}) \quad \forall T \in \mathcal{T}_h. \quad (4.3)$$

Numerical experiments in Section 5 will show that the IFE interpolation function converges to the exact function optimally as the mesh size tends to zero, and this confirms that the IFE spaces developed in this article also have the optimal approximation capability like standard \mathcal{NCRQ}_1 -FE spaces.

4.2. The \mathcal{NCRQ}_1 -IFE Galerkin method

The optimal approximation capability of the \mathcal{NCRQ}_1 -IFE space constructed in Section 2 suggests that we can use it to solve the planar elasticity interface problem (1.1)–(1.4).

Assume that \mathbf{u} solves (1.1)–(1.4) and $\mathbf{u}|_{\Omega^s} \in \mathbf{H}^2(\Omega^s)$, $s = +, -$. Multiplying Eq. (1.1) by $\mathbf{v} \in \mathbf{H}_0^1(\Omega)$ and applying Green's formula on Ω^s , $s = +, -$ leads to:

$$\int_{\Omega^s} 2\mu^s \boldsymbol{\epsilon}(\mathbf{u}) : \boldsymbol{\epsilon}(\mathbf{v}) \, dx dy + \int_{\Omega^s} \lambda^s (\nabla \cdot \mathbf{u})(\nabla \cdot \mathbf{v}) \, dx dy - \int_{\Gamma} \boldsymbol{\sigma}(\mathbf{u}) \mathbf{n} \cdot \mathbf{v} \, ds = \int_{\Omega^s} \mathbf{f} \cdot \mathbf{v} \, dx dy, \quad \forall \mathbf{v} \in \mathbf{H}_0^1(\Omega), \quad (4.4)$$

where the inner-product of two tensors is defined by

$$\boldsymbol{\epsilon}(\mathbf{u}) : \boldsymbol{\epsilon}(\mathbf{v}) = \sum_{ij=1}^2 \epsilon_{ij}(\mathbf{u}) \epsilon_{ij}(\mathbf{v}). \quad (4.5)$$

Summing over s and applying the interface jump condition (1.4), we obtain the following weak form of the planar elasticity interface problem:

$$\int_{\Omega} 2\mu \boldsymbol{\epsilon}(\mathbf{u}) : \boldsymbol{\epsilon}(\mathbf{v}) \, dx dy + \int_{\Omega} \lambda (\nabla \cdot \mathbf{u})(\nabla \cdot \mathbf{v}) \, dx dy = \int_{\Omega} \mathbf{f} \cdot \mathbf{v} \, dx dy, \quad \forall \mathbf{v} \in \mathbf{H}_0^1(\Omega). \quad (4.6)$$

Then the \mathcal{NCRQ}_1 -IFE method in the displacement formulation is given as follows: Find $\mathbf{u}_h \in \mathbf{S}_h(\Omega)$ such that

$$\sum_{T \in \mathcal{T}_h} \int_T 2\mu \boldsymbol{\epsilon}(\mathbf{u}_h) : \boldsymbol{\epsilon}(\mathbf{v}_h) \, dx dy + \sum_{T \in \mathcal{T}_h} \int_T \lambda (\nabla \cdot \mathbf{u}_h)(\nabla \cdot \mathbf{v}_h) \, dx dy = \int_{\Omega} \mathbf{f} \cdot \mathbf{v}_h \, dx dy, \quad \forall \mathbf{v}_h \in \mathbf{S}_h^0(\Omega) \quad (4.7)$$

and

$$\int_e \mathbf{u}_h \, ds = \int_e \mathbf{g} \, ds, \quad \forall e \in \mathcal{E}_h^b,$$

where the \mathcal{NCRQ}_1 -IFE space $\mathbf{S}_h^0(\Omega)$ is defined by

$$\mathbf{S}_h^0(\Omega) = \left\{ \boldsymbol{\Phi} \in \mathbf{S}_h(\Omega) : \int_e \boldsymbol{\Phi} \, ds = \mathbf{0} \text{ if } e \in \mathcal{E}_h^b \right\}. \quad (4.8)$$

5. Numerical experiments

In this section, we use numerical examples to demonstrate features of \mathcal{NCRQ}_1 -IFE method. We investigate the accuracy of both IFE interpolations and IFE solutions with different configurations of interface and Lamé parameters.

We remark that this \mathcal{NCRQ}_1 -IFE Galerkin method can be implemented through the usual finite element procedure. Especially, our numerical experiments suggest that it is unnecessary to use the reduced integration [37] to assemble the algebraic system for this method. In our computations, we use the usual 9-point (3 points in each direction) Gaussian quadrature in all non-interface elements. In each interface element, we partition the two sub-elements formed by the interface into four triangles and carry out integrations on each triangle with the usual 3-point quadrature rule. As demonstrated in the examples presented later in this section, this straightforward implementation of the \mathcal{NCRQ}_1 -IFE Galerkin method performs optimally even if the elasticity material is nearly incompressible.

Let $\Omega = (-1, 1) \times (-1, 1)$ be the solution domain. In all the computations involving IFEs, we use Cartesian meshes \mathcal{T}_h , $h > 0$, which are formed by partitioning Ω into $N \times N$ congruent squares of size $h = 2/N$. To simplify the notation, we let $I_h u_i$, $i = 1, 2$ denote the i -th component of the IFE interpolation $\mathbf{I}_h \mathbf{u}$ of a function \mathbf{u} . Similarly, we use u_{hi} denote the i -th component of the IFE solution \mathbf{u}_h to the interface problem. Errors of an IFE approximation are given in the L^∞ , L^2 , and semi- H^1 norms. In the following error tables, rates of convergence are computed by applying the formulas:

$$\frac{1}{\ln(2)} \ln \left(\frac{\|v_{hj} - u_j\|}{\|u_{h/2,j} - u_j\|} \right), \quad j = 1, 2 \quad (5.1)$$

for a specific norm $\|\cdot\|$, where $v_{hj} = I_h u_j$ or $v_{hj} = u_{hj}$. Errors in the L^∞ norm are defined by

$$\|v_{hj} - u_j\|_{L^\infty} = \max_{T \in \tilde{T}_h} \left(\max_{(x,y) \in T \subset T} |v_{hj}(x,y) - u_j(x,y)| \right), \quad j = 1, 2, \tag{5.2}$$

where, again, $v_{hj} = I_h u_j$ or $v_{hj} = u_{hj}$, and \tilde{T} consists of the 49 uniformly distributed points in T as illustrated in Fig. 7. The L^2 and semi- H^1 norms are computed by suitable Gaussian quadratures.

The first planar elasticity interface problem to be considered has a curve interface Γ that is a circle with radius $r_0 = \pi/8$ subdividing Ω into two sub-domains, denoted by Ω^- and Ω^+ , i.e.,

$$\Omega^- = \{(x,y)^t : x^2 + y^2 < r_0^2\}, \quad \Omega^+ = \{(x,y)^t : x^2 + y^2 > r_0^2\}. \tag{5.3}$$

The boundary function \mathbf{g} and the load function \mathbf{f} in the interface problem (1.1)–(1.4) are chosen such that the exact solution \mathbf{u} is as follows:

$$\mathbf{u}(x,y) = \begin{pmatrix} u_1(x,y) \\ u_2(x,y) \end{pmatrix} = \begin{cases} \begin{pmatrix} u_1^-(x,y) \\ u_2^-(x,y) \end{pmatrix} = \begin{pmatrix} \frac{1}{\lambda^-} r^{\alpha_1} \\ \frac{1}{\lambda^-} r^{\alpha_2} \end{pmatrix} & \text{in } \Omega^-, \\ \begin{pmatrix} u_1^+(x,y) \\ u_2^+(x,y) \end{pmatrix} = \begin{pmatrix} \frac{1}{\lambda^+} r^{\alpha_1} + (\frac{1}{\lambda^-} - \frac{1}{\lambda^+}) r_0^{\alpha_1} \\ \frac{1}{\lambda^+} r^{\alpha_2} + (\frac{1}{\lambda^-} - \frac{1}{\lambda^+}) r_0^{\alpha_2} \end{pmatrix} & \text{in } \Omega^+, \end{cases} \tag{5.4}$$

where $\alpha_1 = 5, \alpha_2 = 7$, and $r = \sqrt{x^2 + y^2}$. Note that this example was discussed in [25].

Example 5.1 (Compressible materials). In this experiment, we test the accuracy of IFE interpolations and IFE solutions for compressible elastic materials, i.e., $\nu^\pm < 0.5$ and ν^\pm is not close to 0.5.

We test three configurations of Lamé parameters which have been investigated by bilinear IFE method in [25]. The first configuration is for a moderate discontinuity in the Lamé parameters, i.e., $\lambda^+ = 5, \lambda^- = 1, \mu^+ = 10, \mu^- = 2$, and Poisson's ratio $\nu^\pm = 1/3$. Corresponding errors in IFE interpolations and IFE solutions are listed in Table 1. The second one is for a larger discontinuity in Lamé parameters, i.e., $\lambda^+ = 100, \lambda^- = 1, \mu^+ = 200, \mu^- = 2$, and Poisson's ratio in this case is $\nu^\pm = 1/3$. Corresponding errors are listed in Table 2. The third one is configured by flipping the Lamé parameters over the sub-domains Ω^- and Ω^+ in the second experiment, i.e., $\lambda^+ = 1, \lambda^- = 100, \mu^+ = 2, \mu^- = 200$, and Poisson's ratio in this case is still $\nu^\pm = 1/3$. Errors of IFE interpolations and IFE solutions are listed in Table 3.

The data in Tables 1–3 suggest that both IFE interpolations and IFE solutions converge optimally in all three norms, i.e.,

$$\|I_h u_i - u_i\|_{L^2} + h \|I_h u_i - u_i\|_{H^1} \approx O(h^2), \quad i = 1, 2, \tag{5.5}$$

$$\|u_{ih} - u_i\|_{L^2} + h \|u_{ih} - u_i\|_{H^1} \approx O(h^2), \quad i = 1, 2. \tag{5.6}$$

Another interesting observation is that the \mathcal{NCRQ}_1 -IFE solution seems to converge optimally in the L^∞ norm, because data in these tables suggest

$$\|u_{ih} - u_i\|_{L^\infty} \approx O(h^2), \quad i = 1, 2. \tag{5.7}$$

Comparing these results with those of linear and bilinear IFE method in [25], we would like to note that while linear and bilinear IFE solutions also converge with optimal rates in L^2 and H^1 norms, they generally have a sub-optimal convergence rate in the L^∞ norm.

Example 5.2 (Nearly incompressible materials). In this experiment, we test the \mathcal{NCRQ}_1 -IFE method for elasticity interface problems with nearly incompressible materials ($\nu \approx 0.5$).

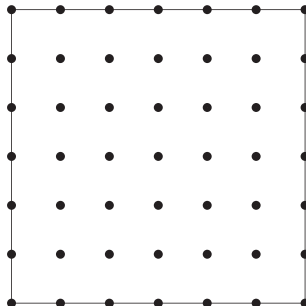


Fig. 7. Points selected to calculate the discrete L^∞ norm on T .

First, we test the problem with a moderate discontinuity in Lamé parameters, i.e., $\lambda^+ = 20, \lambda^- = 1, \mu^+ = 0.02, \mu^- = 0.001$. In this case, Poisson’s ratio $\nu^\pm \approx 0.4995$. We solve this interface problem on the same Cartesian meshes by both the bilinear IFE method proposed in [25] and the \mathcal{NCRQ}_1 -IFE method. Corresponding errors of the IFE solutions are presented in Table 4. Errors of the approximations to the first component u_1 generated by these two IFE methods are also compared in Fig. 8, where the convergence patterns are illustrated more intuitively. The behavior of the approximations to the second component u_2 is similar; hence, we omit the related plots. Then, we compare these two IFE methods with a larger jump in Lamé parameters, i.e., $\lambda^+ = 200, \lambda^- = 1, \mu^+ = 0.2, \mu^- = 0.001$, and $\nu^\pm \approx 0.4995$. Corresponding errors are listed in Table 5.

In our computations for nearly incompressible materials, the \mathcal{NCRQ}_1 -IFE solution \mathbf{u}_h maintains the optimal convergence in the L^∞, L^2 , and H^1 norms. We also note that the \mathcal{NCRQ}_1 solution demonstrates a kind of super-convergence behavior in H^1 norm without any post-processing when the mesh size h is relatively large, but it returns to the usual $O(h)$ order as the mesh becomes finer. Notice that this sort of super-convergence is not visible for compressible materials (see Tables 1–3, for instance) but apparent only for nearly incompressible materials (see also Table 9) at least from our numerical experiments. Also this phenomenon seems to be new compared to the usual super-convergence phenomena observed with suitable post-processing.

In comparison, these experiments clearly demonstrate that the bilinear IFE method suffers the “locking” phenomenon as expected. As the mesh size becomes small, the rates at which the bilinear IFE solution approaches the exact solution are far below the optimal rates in the L^∞, L^2 , and H^1 norms (see data in Tables 4 and 5 and illustrations in Fig. 8). In particular, we

Table 1
Errors of the \mathcal{NCRQ}_1 -IFE solution \mathbf{u}_h with $\lambda^+ = 5, \lambda^- = 1, \mu^+ = 10, \mu^- = 2$ for Example 5.1. The materials are compressible such that $\nu^\pm = 1/3$.

N	$I_h u_1 - u_1$						$I_h u_2 - u_2$					
	$\ \cdot\ _{L^\infty}$	rate	$\ \cdot\ _{L^2}$	rate	$ \cdot _{H^1}$	rate	$\ \cdot\ _{L^\infty}$	rate	$\ \cdot\ _{L^2}$	rate	$ \cdot _{H^1}$	rate
10	5.19E-2		1.76E-2		3.79E-1		1.98E-1		4.52E-2		9.91E-1	
20	1.46E-2	1.83	4.46E-3	1.98	1.91E-1	0.99	5.98E-2	1.72	1.17E-2	1.96	5.06E-1	0.97
40	3.89E-3	1.91	1.12E-3	2.00	9.57E-2	1.00	1.65E-2	1.86	2.93E-3	1.99	2.55E-1	0.99
80	1.00E-3	1.96	2.80E-4	2.00	4.79E-2	1.00	4.32E-3	1.93	7.35E-4	2.00	1.27E-1	1.00
160	2.54E-4	1.98	7.00E-5	2.00	2.40E-2	1.00	1.11E-3	1.97	1.84E-4	2.00	6.37E-2	1.00
320	6.40E-5	1.99	1.75E-5	2.00	1.20E-2	1.00	2.80E-4	1.98	4.59E-5	2.00	3.19E-2	1.00
640	1.61E-5	1.99	4.38E-6	2.00	5.99E-3	1.00	7.05E-5	1.99	1.15E-5	2.00	1.59E-2	1.00
N	$u_{1h} - u_1$						$u_{2h} - u_2$					
	$\ \cdot\ _{L^\infty}$	rate	$\ \cdot\ _{L^2}$	rate	$ \cdot _{H^1}$	rate	$\ \cdot\ _{L^\infty}$	rate	$\ \cdot\ _{L^2}$	rate	$ \cdot _{H^1}$	rate
10	5.76E-2		2.28E-2		4.20E-1		1.98E-1		5.68E-2		1.05E-0	
20	1.79E-2	1.69	5.67E-3	2.00	2.09E-1	1.01	5.90E-2	1.74	1.44E-2	2.00	5.37E-1	0.96
40	5.04E-3	1.83	1.42E-3	2.00	1.04E-1	1.00	1.72E-2	1.78	3.62E-3	2.00	2.70E-1	0.99
80	1.34E-3	1.91	3.54E-4	2.00	5.22E-2	1.00	4.77E-3	1.85	9.05E-4	2.00	1.35E-1	1.00
160	3.44E-4	1.96	8.84E-5	2.00	2.61E-2	1.00	1.25E-3	1.93	2.26E-4	2.00	6.77E-2	1.00
320	8.73E-5	1.98	2.21E-5	2.00	1.31E-2	1.00	3.22E-4	1.96	5.66E-5	2.00	3.38E-2	1.00
640	2.20E-5	1.99	5.52E-6	2.00	6.53E-3	1.00	8.15E-5	1.98	1.41E-5	2.00	1.69E-2	1.00

Table 2
Errors of the \mathcal{NCRQ}_1 -IFE solution \mathbf{u}_h with $\lambda^+ = 100, \lambda^- = 1, \mu^+ = 200, \mu^- = 2$ for Example 5.1. The materials are compressible such that $\nu^\pm = 1/3$.

N	$I_h u_1 - u_1$						$I_h u_2 - u_2$					
	$\ \cdot\ _{L^\infty}$	rate	$\ \cdot\ _{L^2}$	rate	$ \cdot _{H^1}$	rate	$\ \cdot\ _{L^\infty}$	rate	$\ \cdot\ _{L^2}$	rate	$ \cdot _{H^1}$	rate
10	2.59E-3		1.20E-3		2.52E-2		9.88E-3		2.26E-3		4.97E-2	
20	9.70E-4	1.41	3.16E-4	1.93	1.36E-2	0.89	2.99E-3	1.72	5.84E-4	1.96	2.54E-2	0.97
40	3.46E-4	1.49	8.29E-5	1.93	7.13E-3	0.93	8.24E-4	1.86	1.47E-4	1.99	1.28E-2	0.99
80	9.64E-5	1.84	2.13E-5	1.96	3.66E-3	0.96	2.16E-4	1.93	3.69E-5	2.00	6.41E-3	1.00
160	2.55E-5	1.92	5.44E-6	1.97	1.86E-3	0.98	5.54E-5	1.97	9.24E-6	2.00	3.21E-3	1.00
320	6.55E-6	1.96	1.37E-6	1.99	9.37E-4	0.99	1.40E-5	1.98	2.31E-6	2.00	1.60E-3	1.00
640	1.68E-6	1.96	3.45E-7	1.99	4.70E-4	0.99	3.52E-6	1.99	5.78E-7	2.00	8.02E-4	1.00
N	$u_{1h} - u_1$						$u_{2h} - u_2$					
	$\ \cdot\ _{L^\infty}$	rate	$\ \cdot\ _{L^2}$	rate	$ \cdot _{H^1}$	rate	$\ \cdot\ _{L^\infty}$	rate	$\ \cdot\ _{L^2}$	rate	$ \cdot _{H^1}$	rate
10	3.54E-3		1.80E-3		2.65E-2		9.88E-3		2.91E-3		5.26E-2	
20	1.15E-3	1.63	4.58E-4	1.97	1.44E-2	0.87	2.95E-3	1.74	7.38E-4	1.98	2.70E-2	0.96
40	3.42E-4	1.74	1.22E-4	1.90	7.65E-3	0.92	8.59E-4	1.78	1.86E-4	1.99	1.36E-2	0.99
80	1.12E-4	1.61	3.07E-5	1.99	3.95E-3	0.95	2.38E-4	1.85	4.64E-5	2.00	6.82E-3	1.00
160	3.20E-5	1.81	7.66E-6	2.00	2.01E-3	0.98	6.27E-5	1.93	1.16E-5	2.00	3.41E-3	1.00
320	8.57E-6	1.90	1.90E-6	2.01	1.01E-3	0.99	1.61E-5	1.96	2.90E-6	2.00	1.70E-3	1.00
640	2.24E-6	1.94	4.79E-7	1.99	5.08E-4	0.99	4.07E-6	1.98	7.24E-7	2.00	8.52E-4	1.00

Table 3

Errors of the \mathcal{NCRQ}_1 -IFE solution \mathbf{u}_h with $\lambda^+ = 1, \lambda^- = 100, \mu^+ = 2, \mu^- = 200$ for Example 5.1. The materials are compressible such that $\nu^\pm = 1/3$.

N	$I_h u_1 - u_1$						$I_h u_2 - u_2$					
	$\ \cdot\ _{L^\infty}$	rate	$\ \cdot\ _{L_2}$	rate	$ \cdot _{H_1}$	rate	$\ \cdot\ _{L^\infty}$	rate	$\ \cdot\ _{L_2}$	rate	$ \cdot _{H_1}$	rate
10	2.59E-1		8.79E-2		1.89E-0		9.88E-1		2.26E-1		4.95E-0	
20	7.32E-2	1.83	2.23E-2	1.98	9.53E-1	0.99	2.99E-1	1.72	5.82E-2	1.96	2.53E-0	0.97
40	1.94E-2	1.91	5.58E-3	2.00	4.78E-1	1.00	8.24E-2	1.86	1.47E-2	1.99	1.27E-0	0.99
80	5.01E-3	1.96	1.40E-3	2.00	2.29E-1	1.00	2.16E-2	1.93	3.67E-3	2.00	6.37E-1	1.00
160	1.27E-3	1.98	3.49E-4	2.00	1.20E-1	1.00	5.54E-3	1.97	9.19E-4	2.00	3.19E-1	1.00
320	3.20E-4	1.99	8.73E-5	2.00	5.98E-2	1.00	1.40E-3	1.98	2.30E-4	2.00	1.59E-1	1.00
640	8.03E-5	1.99	2.18E-5	2.00	2.99E-2	1.00	3.52E-4	1.99	5.74E-5	2.00	7.97E-2	1.00

N	$u_{1h} - u_1$						$u_{2h} - u_2$					
	$\ \cdot\ _{L^\infty}$	rate	$\ \cdot\ _{L_2}$	rate	$ \cdot _{H_1}$	rate	$\ \cdot\ _{L^\infty}$	rate	$\ \cdot\ _{L_2}$	rate	$ \cdot _{H_1}$	rate
10	2.88E-1		1.11E-1		2.07E-0		9.87E-1		2.82E-1		5.23E-0	
20	8.95E-2	1.67	2.77E-2	2.00	1.04E-0	0.99	2.95E-1	1.74	7.16E-2	1.98	2.69E-0	0.96
40	2.52E-2	1.83	6.92E-3	2.00	5.21E-1	1.00	8.58E-2	1.78	1.80E-2	2.00	1.35E-0	0.90
80	6.68E-3	1.91	1.73E-3	2.00	2.61E-1	1.00	2.38E-2	1.85	4.50E-3	2.00	6.77E-1	1.00
160	1.72E-3	1.96	4.32E-4	2.00	1.30E-1	1.00	6.27E-3	1.93	1.12E-3	2.00	3.38E-1	1.00
320	4.37E-4	1.98	1.08E-4	2.00	6.51E-2	1.00	1.61E-3	1.96	2.81E-4	2.00	1.69E-1	1.00
640	1.10E-4	1.99	2.70E-5	2.00	3.26E-2	1.00	4.07E-4	1.98	7.02E-5	2.00	8.46E-2	1.00

Table 4

Comparison of errors in the bilinear IFE solution and the \mathcal{NCRQ}_1 -IFE solution in “Locking” test with $\lambda^+ = 20, \lambda^- = 1, \mu^+ = 0.02, \mu^- = 0.001$ for Example 5.2. The materials are nearly incompressible such that $\nu^\pm \approx 0.4995$.

N	$u_{1h} - u_1$						$u_{2h} - u_2$					
	$\ \cdot\ _{L^\infty}$	rate	$\ \cdot\ _{L_2}$	rate	$ \cdot _{H_1}$	rate	$\ \cdot\ _{L^\infty}$	rate	$\ \cdot\ _{L_2}$	rate	$ \cdot _{H_1}$	rate
<i>Bilinear IFE method</i>												
10	2.18 E-2		1.89 E-2		1.28 E-1		4.18 E-2		3.00 E-2		2.49 E-1	
20	1.53 E-2	0.51	1.27 E-2	0.57	9.39 E-2	0.44	2.44 E-2	0.51	2.06 E-2	0.54	1.63 E-1	0.62
40	8.74 E-3	0.80	7.02 E-3	0.85	5.82 E-2	0.69	1.42 E-2	0.78	1.20 E-2	0.78	9.09 E-2	0.84
80	4.14 E-3	1.08	2.94 E-3	1.26	3.18 E-2	0.87	6.48 E-3	1.13	4.88 E-3	1.29	4.37 E-2	1.06
160	1.85 E-3	1.17	9.99 E-4	1.56	1.62 E-2	0.98	2.34 E-3	1.47	1.68 E-3	1.54	2.16 E-2	1.02
320	8.47 E-4	1.12	3.55 E-4	1.49	8.91 E-3	0.86	1.62 E-3	0.53	5.96 E-4	1.49	1.39 E-2	0.63
640	7.01 E-4	0.27	1.96 E-4	0.86	6.51 E-3	0.45	9.51 E-4	0.77	2.93 E-4	1.02	8.54 E-3	0.70
1280	3.75 E-4	0.90	1.03 E-4	0.93	4.29 E-3	0.60	4.16 E-4	1.19	1.50 E-4	0.97	5.14 E-3	0.73
<i>Nonconforming rotated Q_1 IFE method</i>												
10	1.76 E-1		5.08 E-2		6.50 E-1		9.69 E-2		3.92 E-2		5.36 E-1	
20	6.21 E-2	1.50	1.70 E-2	1.57	2.91 E-1	1.16	7.44 E-2	0.38	1.48 E-2	1.41	3.77 E-1	0.51
40	2.60 E-2	1.26	5.78 E-3	1.56	1.45 E-1	1.01	4.23 E-2	0.81	5.27 E-3	1.49	2.18 E-1	0.79
80	8.02 E-3	1.70	1.65 E-3	1.81	5.80 E-2	1.32	1.46 E-2	1.54	1.53 E-3	1.78	9.55 E-2	1.19
160	2.14 E-3	1.91	4.40 E-4	1.91	2.24 E-2	1.37	4.39 E-3	1.73	4.12 E-4	1.90	3.82 E-2	1.32
320	5.77 E-4	1.92	1.15 E-4	1.94	9.07 E-3	1.30	1.20 E-3	1.87	1.08 E-4	1.94	1.57 E-2	1.28
640	1.43 E-4	2.01	2.91 E-5	1.98	3.86 E-3	1.23	3.11 E-4	1.95	2.74 E-5	1.97	6.73 E-3	1.22
1280	3.83 E-5	1.90	7.33 E-6	1.99	1.73 E-3	1.16	8.08 E-5	1.94	6.92 E-6	1.99	3.02 E-3	1.16

have not even observed the bilinear IFE solution to have any obvious convergence pattern in the L^∞ norm. Therefore, these experiments strongly suggest that the \mathcal{NCRQ}_1 -IFE method is more reliable because of its desirable “locking-free” feature for solving the elasticity interface problems.

We now consider another interface problem described by (1.1)–(1.4) in which the interface is a straight line. Specifically, we assume that the interface Γ is a vertical straight line $x = x_0$ that divides the solution domain $\Omega = (-1, 1) \times (-1, 1)$ into two sub-domains, denoted by Ω^- and Ω^+ , i.e.,

$$\Omega^- = \{(x, y)^t \in \Omega : x < x_0\}, \quad \Omega^+ = \{(x, y)^t \in \Omega : x > x_0\}. \tag{5.8}$$

The boundary condition function \mathbf{g} and the load function \mathbf{f} in this interface problem are chosen such that the exact solution \mathbf{u} is as follows:

$$\mathbf{u}(x, y) = \begin{pmatrix} u_1(x, y) \\ u_2(x, y) \end{pmatrix} = \begin{cases} \begin{pmatrix} u_1^-(x, y) \\ u_2^-(x, y) \end{pmatrix} = \begin{pmatrix} \frac{1}{\lambda^- + 2\mu^-} (x - x_0) \cos(2xy) \\ \frac{1}{\mu^-} (x - x_0) \cos(2xy) \end{pmatrix} & \text{in } \Omega^-, \\ \begin{pmatrix} u_1^+(x, y) \\ u_2^+(x, y) \end{pmatrix} = \begin{pmatrix} \frac{1}{\lambda^+ + 2\mu^+} (x - x_0) \cos((x + x_0)y) \\ \frac{1}{\mu^+} (x - x_0) \cos((x + x_0)y) \end{pmatrix} & \text{in } \Omega^+. \end{cases} \tag{5.9}$$

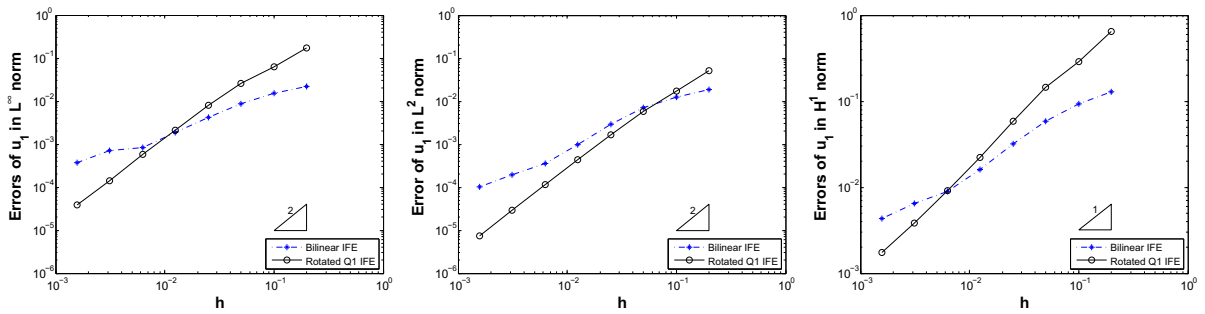


Fig. 8. Comparison of errors of the bilinear IFE and the \mathcal{NCRQ}_1 -IFE solutions to u_1 for Example 5.2. From left to right: L^∞ norm error, L^2 norm error, H^1 norm error.

Table 5

Comparison of errors in the bilinear IFE solution and the \mathcal{NCRQ}_1 -IFE solution in “Locking” test with $\lambda^+ = 200, \lambda^- = 1, \mu^+ = 0.2, \mu^- = 0.001$ for Example 5.2. The materials are compressible such that $\nu^\pm \approx 0.4995$.

N	$u_{1h} - u_1$				$u_{2h} - u_2$							
	$\ \cdot\ _{L^\infty}$	rate	$\ \cdot\ _{L^2}$	rate	$ \cdot _{H^1}$	rate	$\ \cdot\ _{L^\infty}$	rate	$\ \cdot\ _{L^2}$	rate	$ \cdot _{H^1}$	rate
<i>Bilinear IFE method</i>												
10	3.74E-3		2.37E-3		2.05E-2		4.18E-3		3.11E-3		2.55E-2	
20	4.07E-3	-.12	1.69E-3	0.49	2.11E-2	-.04	4.40E-3	-.07	2.20E-3	0.49	1.99E-2	0.36
40	3.66E-3	0.15	1.49E-3	0.18	2.03E-2	0.05	3.64E-3	0.28	1.41E-3	0.65	1.57E-2	0.35
80	3.53E-3	0.05	1.24E-3	0.27	1.97E-2	0.05	3.12E-3	0.22	8.96E-4	0.65	1.37E-2	0.19
160	1.93E-3	0.87	6.00E-4	1.05	1.27E-2	0.63	1.59E-3	0.97	4.41E-4	1.02	1.14E-2	0.27
320	6.97E-4	1.47	2.22E-4	1.44	6.05E-3	1.07	8.34E-4	0.93	1.64E-4	1.43	6.35E-3	0.84
640	3.83E-4	0.86	6.48E-5	1.77	3.58E-3	0.76	3.26E-4	1.36	6.18E-5	1.41	4.04E-3	0.65
1280	1.93E-4	0.99	2.42E-5	1.42	2.44E-3	0.55	1.61E-4	1.02	2.83E-5	1.13	2.88E-3	0.49
<i>Nonconforming rotated Q1 IFE method</i>												
10	6.43E-2		1.50E-2		2.19E-1		2.99E-2		7.01E-3		1.08E-1	
20	2.11E-2	1.61	5.91E-3	1.34	1.01E-1	1.12	2.49E-2	0.14	3.83E-3	0.87	1.03E-1	0.06
40	1.51E-2	0.48	3.15E-3	0.91	7.99E-2	0.34	2.15E-2	0.21	2.71E-3	0.50	1.05E-1	-.03
80	6.20E-3	1.29	1.40E-3	1.17	4.32E-2	0.89	1.23E-2	0.81	1.26E-3	1.10	6.59E-2	0.67
160	1.87E-3	1.73	4.39E-4	1.68	1.75E-2	1.30	4.11E-3	1.58	4.01E-4	1.65	2.91E-2	1.18
320	5.27E-4	1.83	1.17E-4	1.91	6.60E-3	1.41	1.15E-3	1.83	1.08E-4	1.90	1.11E-2	1.39
640	1.45E-4	1.86	3.04E-5	1.94	2.44E-3	1.43	3.05E-4	1.92	2.82E-5	1.93	4.13E-3	1.43
1280	3.77E-5	1.95	7.73E-6	1.98	8.94E-4	1.45	7.90E-5	1.95	7.18E-6	1.97	1.49E-3	1.47

Example 5.3 (Solving a group of interface problems on the same mesh). In this experiment, to demonstrate the advantage and robustness of the \mathcal{NCRQ}_1 -IFE method, we use one mesh to solve 5 elasticity interface problems whose interfaces are straight lines located at

$$x_0 = -\frac{\pi}{100}, -\frac{\pi}{200}, 0, \frac{\pi}{200}, \frac{\pi}{100},$$

respectively.

The Cartesian mesh formed in $\Omega = (-1, 1) \times (-1, 1)$ for this experiment has the mesh size $h = 2/320$. The Lamé parameters of the elasticity interface problem in this experiment are $\lambda^+ = 2, \lambda^- = 1, \mu^+ = 3, \mu^- = 2$ representing a typical compressible material configuration with a moderate jump. Errors of IFE solutions generated on this fixed mesh to these interface problems are listed in Table 6. Since the data presented in this table clearly indicate that IFE solutions to all of these interface problems have comparable accuracy in the L^∞, L^2 , and semi- H^1 norms even though the interfaces in these problems are at different locations, the IFE method proposed here is potentially advantageous in applications that require to solve elasticity interface problems with a sequence of material interfaces.

In addition, for those problems whose straight line interfaces are at

$$x_0 = -\frac{\pi}{100}, -\frac{\pi}{200}, \frac{\pi}{200}, \frac{\pi}{100},$$

respectively, we note that the mesh contains interface elements and IFE functions developed in Section 2 are used in generating solutions to these interface problems. However, for the problem whose interface is at $x_0 = 0$, the interface coincides

Table 6

Errors of the \mathcal{NCRQ}_1 -IFE solutions \mathbf{u}_h for problems whose interfaces are at different locations for Example 5.3. The mesh size is $h = 2/320$ and the Lamé parameters are $\lambda^+ = 2, \lambda^- = 1, \mu^+ = 3, \mu^- = 2$. The materials are compressible such that $\nu^+ = 0.2, \nu^- \approx 0.1667$.

Interface location:	$u_{1h} - u_1$			$u_{2h} - u_2$		
	$\ \cdot\ _{L^\infty}$	$\ \cdot\ _{L^2}$	$ \cdot _{H^1}$	$\ \cdot\ _{L^\infty}$	$\ \cdot\ _{L^2}$	$ \cdot _{H^1}$
$-\pi/100$	1.1777E-5	2.5923E-6	1.7824E-3	2.4343E-5	7.3793E-6	4.3019E-3
$-\pi/200$	1.1887E-5	2.6252E-6	1.8043E-3	2.4573E-5	7.4702E-6	4.3544E-3
0	1.1997E-5	2.6583E-6	1.8263E-3	2.4803E-5	7.5610E-6	4.4070E-3
$\pi/200$	1.2107E-5	2.6915E-6	1.8483E-3	2.5034E-5	7.6520E-6	4.4597E-3
$\pi/100$	1.2218E-5	2.7249E-6	1.8703E-3	2.5264E-5	7.7430E-6	4.5123E-3

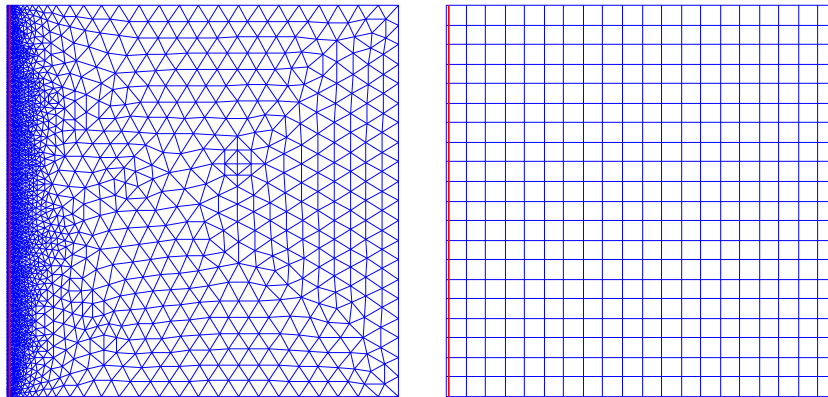


Fig. 9. Different meshes are compared for the Thin Layer Interface Problem 5.4. The left plot is a body-fitting triangular mesh which has 5128 triangles. The right plot is a non-body-fitting Cartesian mesh which contains 400 rectangles.

with edges of those elements besides the vertical interface line $x = 0$. In this case, the mesh has no interface elements so that the \mathcal{NCRQ}_1 -IFE method is in fact the \mathcal{NCRQ}_1 -FE method according to the consistency of the \mathcal{NCRQ}_1 -IFE functions as stated in Lemma 3.3. The errors data in Table 6 confirm that the IFE method can perform as accurately as the FE method, but the IFE method has the advantage that its mesh does not have to be generated according to the interface location.

Example 5.4 (IFE solution for a problem with a boundary layer). In this experiment, we assume that a straight line interface is located at $x_0 = -1 + \pi/300$. Since the interface $x = -1 + \pi/300$ is very close the left boundary of Ω , the sub-domain Ω^- is a very thin layer beside the left boundary of Ω .

If we use the standard FE method to solve this interface problem, then the body-fitting restriction requires the elements inside Ω^- and around the interface to be very small so that they can be placed entirely inside or outside of the thin layer, but not to be cut by the interface. Generating a body-fitting mesh for a solution domain with a boundary layer is not only complicated, but also leads to an unstructured mesh with a large number of degrees of freedom usually. Since an IFE method allows interfaces to be embedded in finite elements, a simple Cartesian mesh with much less degrees of freedom can be used for solving the same interface problem in which one of the materials forms a thin layer of the solution domain. Fig. 9 provides a comparison of these two types of meshes for the thin layer interface problem. The unstructured mesh in Fig. 9 has 5128 triangular elements. When this mesh is used together with the standard linear FEs to solve our elasticity interface problem, the global degrees of freedom in the FE system is 5402. On the other hand, the structured mesh in Fig. 9 has only 400 rectangular elements, on which the global degrees of freedom in the \mathcal{NCRQ}_1 -IFE method are 1600, much less than those of the FE method. Most importantly, the error data in Table 7 demonstrate that the accuracies of solutions obtained by smaller IFE systems and by the much larger FE system are not much different. Therefore, the IFE method has its advantage over the FE method for interface problems with thin layers.

We then investigate the convergence of the \mathcal{NCRQ}_1 -IFE method for thin layer case in which the interface is the vertical line at $x_0 = -1 + \pi/300$. We test for both compressible ($\lambda^+ = 2, \lambda^- = 1, \mu^+ = 3, \mu^- = 2, \nu^+ = 0.2, \nu^- \approx 0.1667$) and the nearly incompressible ($\lambda^+ = 2000, \lambda^- = 1000, \mu^+ = 3, \mu^- = 1, \nu^+ \approx 0.4993, \nu^- \approx 0.4995$) materials. Errors of IFE solutions are listed in Tables 8 and 9. These numerical results indicate that the \mathcal{NCRQ}_1 -IFE method can solve the thin layer elasticity interface problem optimally in L^∞, L^2 and H^1 norms for both compressible and nearly incompressible materials. In Fig. 10, we plot error data in different norms for the incompressible material configuration for an illustration of the convergence behavior.

We note that, in the computations on those meshes whose mesh sizes are

Table 7

Comparison of errors of the linear FE and \mathcal{NCRQ}_1 -IFE solutions \mathbf{u}_h for the Thin Layer Example 5.4. The Lamé parameters are $\lambda^+ = 2, \lambda^- = 1, \mu^+ = 3, \mu^- = 2$ so that the material is compressible such that $\nu^+ = 0.2, \nu^- \approx 0.1667$.

Method	$u_{1h} - u_1$			$u_{2h} - u_2$		
	$\ \cdot\ _{L^\infty}$	$\ \cdot\ _{L_2}$	$ \cdot _{H_1}$	$\ \cdot\ _{L^\infty}$	$\ \cdot\ _{L_2}$	$ \cdot _{H_1}$
FE method	3.61E-4	2.38E-4	7.17E-3	7.16E-4	5.53E-4	1.89E-2
IFE method	8.70E-4	1.97E-4	8.42E-3	1.96E-4	5.34E-4	2.20E-2

Table 8

Errors of the \mathcal{NCRQ}_1 -IFE solution \mathbf{u}_h with $\lambda^+ = 2, \lambda^- = 1, \mu^+ = 3, \mu^- = 2$ for Example 5.4. The materials are compressible such that $\nu^+ = 0.2, \nu^- \approx 0.1667$.

N	$u_{1h} - u_1$						$u_{2h} - u_2$					
	$\ \cdot\ _{L^\infty}$	rate	$\ \cdot\ _{L_2}$	rate	$ \cdot _{H_1}$	rate	$\ \cdot\ _{L^\infty}$	rate	$\ \cdot\ _{L_2}$	rate	$ \cdot _{H_1}$	rate
10	3.15E-3		7.52E-4		1.68E-2		7.40E-3		2.03E-3		4.38E-2	
20	8.70E-4	1.86	1.97E-4	1.94	8.42E-3	1.00	1.96E-3	1.92	5.34E-4	1.93	2.20E-2	1.00
40	2.37E-4	1.87	5.07E-5	1.95	4.22E-3	1.00	5.36E-4	1.87	1.38E-4	1.95	1.10E-2	1.00
80	7.09E-5	1.74	1.30E-5	1.97	2.12E-3	0.99	1.53E-4	1.81	3.51E-5	1.97	5.52E-3	0.99
160	2.32E-5	1.61	3.24E-6	2.00	1.07E-3	0.99	4.61E-5	1.73	8.76E-6	2.00	2.78E-3	0.99
320	5.95E-6	1.97	8.18E-7	1.98	5.34E-4	1.00	1.28E-5	1.85	2.22E-6	1.98	1.39E-3	1.00
640	1.48E-6	2.01	2.04E-7	2.00	2.67E-4	1.00	3.38E-6	1.92	5.54E-7	2.00	6.94E-4	1.00

Table 9

Errors of the \mathcal{NCRQ}_1 -IFE solution \mathbf{u}_h with $\lambda^+ = 2000, \lambda^- = 1000, \mu^+ = 3, \mu^- = 1$ for Example 5.4. The materials are nearly incompressible such that $\nu^+ \approx 0.4995, \nu^- \approx 0.4993$.

N	$u_{1h} - u_1$						$u_{2h} - u_2$					
	$\ \cdot\ _{L^\infty}$	rate	$\ \cdot\ _{L_2}$	rate	$ \cdot _{H_1}$	rate	$\ \cdot\ _{L^\infty}$	rate	$\ \cdot\ _{L_2}$	rate	$ \cdot _{H_1}$	rate
10	7.63E-2		6.63E-2		2.56E-1		8.86E-2		6.98E-2		2.89E-1	
20	1.83E-2	2.06	1.69E-2	1.97	6.76E-2	1.92	2.26E-3	1.97	1.78E-2	1.98	7.71E-2	1.91
40	4.69E-3	1.96	4.41E-3	1.94	1.93E-2	1.81	5.66E-3	2.00	4.52E-3	1.97	2.26E-2	1.77
80	1.23E-3	1.93	1.19E-3	1.89	6.58E-3	1.55	1.45E-3	1.96	1.17E-3	1.95	8.72E-3	1.37
160	3.23E-4	1.93	3.20E-4	1.90	2.81E-3	1.23	3.71E-4	1.97	3.07E-4	1.94	4.05E-3	1.11
320	8.00E-5	2.01	7.88E-5	2.02	1.29E-4	1.12	9.23E-5	2.01	7.59E-5	2.01	1.74E-3	1.22
640	1.98E-5	2.01	1.95E-5	2.02	6.31E-4	1.03	2.30E-5	2.01	1.88E-5	2.01	8.39E-4	1.05
1280	4.99E-6	1.99	4.91E-6	1.99	3.16E-4	1.00	5.76E-6	2.00	4.74E-6	1.99	4.17E-4	1.01

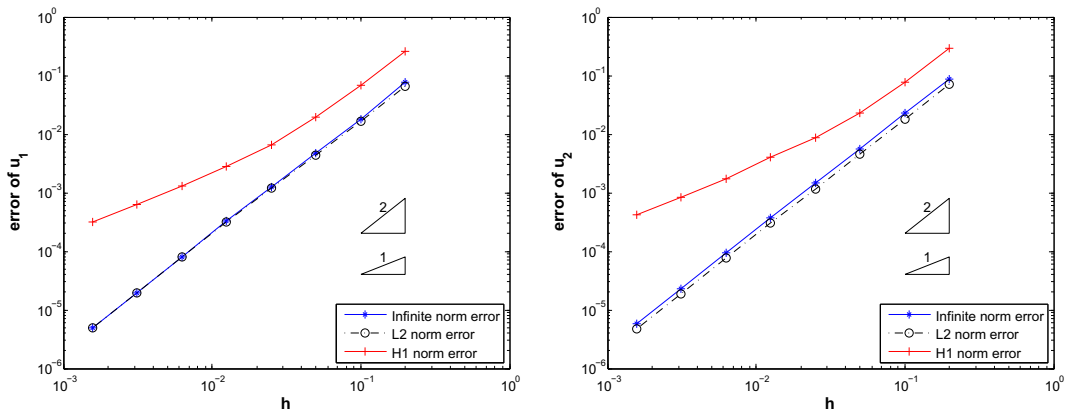


Fig. 10. Plots of errors of IFE solutions \mathbf{u}_h for the Thin Layer Example 5.4 in different norms. The left and right plots are for the first component u_1 and the second component u_2 , respectively.

$$h = 2/10, 2/20, 2/40, 2/80, 2/160,$$

the interface $x = -1 + \pi/300$ is in the first layer of elements adjacent to the left boundary of $\Omega = (-1, 1) \times (-1, 1)$. But on those meshes whose mesh sizes are $2/320$ and smaller, the interface line is not in the first layer of elements on the left anymore. This property demonstrates the robustness of this IFE method from the point of view of the interface location in a mesh.

Table 10

Errors of nonconforming rotated Q_1 IFE solution \mathbf{u}_h for Example 5.5 with $\lambda^+ = 2000, \lambda^- = 1000, \mu^+ = 3, \mu^- = 1, \nu^+ \approx 0.4993,$ and $\nu^- \approx 0.4995$.

N	$u_{1h} - u_1$			$u_{2h} - u_2$								
	$\ \cdot\ _{L^\infty}$	rate	$\ \cdot\ _{L^2}$	rate	$ \cdot _{H^1}$	rate	$\ \cdot\ _{L^\infty}$	rate	$\ \cdot\ _{L^2}$	rate	$ \cdot _{H^1}$	rate
10	$8.11E-1$		$7.05E-1$		$2.76E-0$		$1.20E-0$		$7.25E-1$		$3.21E-0$	
20	$2.01E-1$	2.01	$1.78E-1$	1.99	$7.11E-1$	1.96	$2.73E-1$	2.13	$1.82E-1$	2.00	$8.25E-1$	1.96
40	$4.98E-2$	2.01	$4.46E-2$	2.00	$1.85E-1$	1.94	$6.78E-2$	2.01	$4.54E-2$	2.00	$2.17E-1$	1.92
80	$1.24E-2$	2.00	$1.12E-2$	2.00	$5.23E-2$	1.82	$1.69E-2$	2.00	$1.14E-3$	2.00	$6.37E-2$	1.77
160	$3.11E-3$	2.00	$2.79E-3$	2.00	$1.79E-2$	1.55	$4.24E-3$	2.00	$2.84E-3$	2.00	$2.30E-2$	1.47
320	$7.77E-4$	2.00	$6.98E-4$	2.00	$7.54E-3$	1.24	$1.06E-4$	2.00	$7.10E-4$	2.00	$1.01E-2$	1.19
640	$1.94E-4$	2.00	$1.74E-4$	2.00	$3.58E-3$	1.08	$2.65E-4$	2.00	$1.77E-4$	2.00	$4.85E-3$	1.06
1280	$4.86E-5$	2.00	$4.36E-5$	2.00	$1.76E-3$	1.02	$6.62E-5$	2.00	$4.43E-5$	2.00	$2.40E-3$	1.01

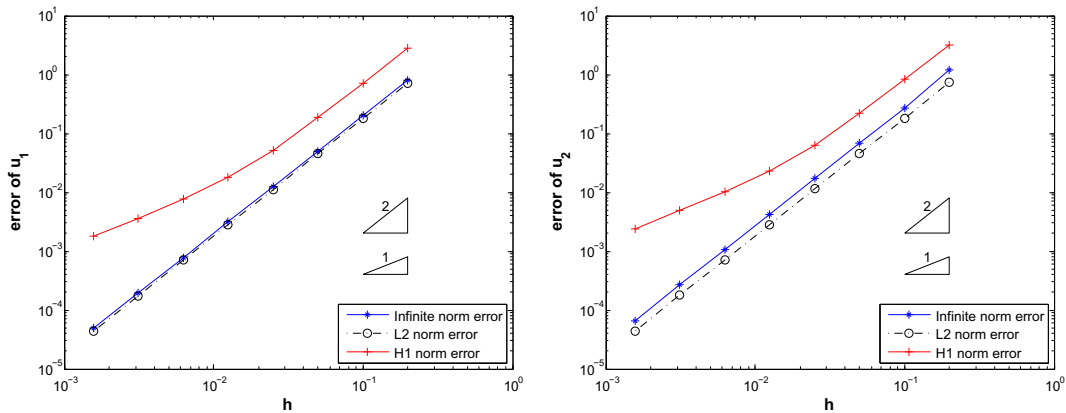


Fig. 11. These plots are errors of IFE solutions \mathbf{u}_h in different norms for Example 5.5. The left plot is for the first component u_1 and the right plot is for the second component u_2 .

From the errors in H^1 norm for a nearly incompressible case in Table 9, one can observe a kind of super-convergence behavior with coarse meshes, but the convergence rate tends to be an optimal $O(h)$ order as the meshes become finer. This phenomenon is also observed in the nearly incompressible case of Example 5.2.

Example 5.5 (*Reduced quadrature is unnecessary on rectangular meshes*). Even though a reduced quadrature procedure is used to prevent the numerical locking for the $NCRQ_1$ -FE method on general quadrilateral meshes [37], this example intends to demonstrate that, on rectangular meshes, both the $NCRQ_1$ -FE and $NCRQ_1$ -IFE methods without any special quadrature procedure do not seem to have the locking shortcoming.

In this example, the straight line interface is $x = 1/640$. Nearly incompressible materials are chosen such that $\lambda^+ = 2000, \lambda^- = 1000, \mu^+ = 3, \mu^- = 1, \nu^+ \approx 0.4993,$ and $\nu^- \approx 0.4995$. The error data listed in Table 10 demonstrate that the $NCRQ_1$ -IFE method converges optimally in the L^∞, L^2 and H^1 norms even though the standard quadrature procedures described at the beginning of this section are used in all computations to generate these numerical results. Plots in Fig. 11 further illustrate the convergence features of the $NCRQ_1$ -IFE method. Again, we remark that the $NCRQ_1$ -IFE method possesses a certain superconvergence in the H^1 norm on coarse meshes, but on finer meshes, it converges at the optimal order dictated by the polynomials used in this method. Furthermore, the mesh corresponding to $N = 1280$ has no interface elements and the $NCRQ_1$ -IFE solution produced on this mesh is the $NCRQ_1$ -FE solution because of the consistency of the $NCRQ_1$ -IFE functions stated in Lemma 3.3. These data clearly suggests that, both the $NCRQ_1$ -FE and $NCRQ_1$ -IFE methods are locking free on rectangular meshes without using any special quadrature procedure.

6. Conclusion

In this article, we have proposed a new IFE method based on the $NCRQ_1$ finite element for solving planar elasticity interface problems with discontinuous Lamé parameters. This method can be used on Cartesian meshes even if the material interface is nontrivial. We prove that the nonconforming IFE basis functions can be constructed for any configuration of the elasticity materials and interface geometry. Our numerical experiments indicate that the $NCRQ_1$ -IFE solution has the optimal convergence in L^2, H^1 and L^∞ norms. The method is robust in the sense that it does not suffer from the dreaded volume “locking”. This IFE method can solve a sequence/group of interface problems by one mesh so long as their interface are not

drastically different in topology. In addition, this IFE method can use simple Cartesian meshes to effectively and reliably solve interface problems with thin boundary layers. We note that there have been published results [36] concerning the $\mathcal{NCR}Q_1$ finite element methods for the 3D elasticity system, but, to our best knowledge, no published results yet for using $\mathcal{NCR}Q_1$ -IFE to solve elasticity interface problems. The ideas in this article seem to be readily extendable to the 3D case; however, classifying the location of interface relative to the faces of a cubic element is an issue far more complicated than its 2D counterpart. It is therefore an interesting future research topic to extend this nonconforming rotated IFE method to the three dimensional elasticity interface problems.

Acknowledgement

We are very grateful for the constructive suggestions and comments provided by both referees that greatly helped us improve the presentation of our research in the revision of this manuscript.

References

- [1] M.P. Bendsøe, O. Sigmund, *Topology Optimization Theory, Methods and Applications*, Springer, 2003.
- [2] L.V. Gibiansky, O. Sigmund, Multiphase composites with extremal bulk modulus, *J. Mech. Phys. Solids* 48 (3) (2000) 461–498.
- [3] O. Sigmund, Design of multiphysics actuators using topology optimization Part II: two-material structures, *Comput. Methods Appl. Mech. Eng.* 190 (49–50) (2001) 6605–6627.
- [4] H.J. Jou, P.H. Leo, J.S. Lowengrub, Microstructural evolution in inhomogeneous elastic media, *J. Comput. Phys.* 131 (1) (1997) 109–148.
- [5] P.H. Leo, J.S. Lowengrub, Q. Nie, Microstructural evolution in orthotropic elastic media, *J. Comput. Phys.* 157 (1) (2000) 44–88.
- [6] H. Gao, Y. Huang, F.F. Abraham, Continuum and atomistic studies of intersonic crack propagation, *J. Mech. Phys. Solids* 49 (9) (2001) 2113–2132.
- [7] A.P. Sutton, R.W. Balluffi, *Interfaces in Crystalline Materials*, Oxford Science Publications, 1995.
- [8] S.C. Brenner, L.R. Scott, *The Mathematical Theory of Finite Element Methods*, Springer-Verlag, New York, 1994.
- [9] P.G. Ciarlet, *Mathematical Elasticity, Volume I: Three-dimensional elasticity*, Studies in mathematics and its applications, vol. 20, North-Holland Publishing Co., Amsterdam, 1998.
- [10] O.C. Zienkiewicz, R.L. Taylor, *The Finite Element Method, Solid Mechanics*, vol. 2, Butterworth-Heinemann, 2000.
- [11] I. Babuška, The finite element method for elliptic equations with discontinuous coefficients, *Computing* 5 (1970) 207–213.
- [12] X. Yang, Immersed interface method for elasticity problems with interfaces, Ph.D. thesis, North Carolina State University, 2004.
- [13] X. Yang, B. Li, Z. Li, The immersed interface method for elasticity problems with interfaces, *Dyn. Contin. Discrete Impuls. Syst. Ser. A Math. Anal.* 10 (5) (2003) 783–808.
- [14] A. Hansbo, P. Hansbo, A finite element method for the simulation of strong and weak discontinuities in solid mechanics, *Comput. Methods Appl. Mech. Eng.* 193 (33–35) (2004) 3523–3540.
- [15] R. Becker, E. Burman, P. Hansbo, A Nitsche extended finite element method for incompressible elasticity with discontinuous modulus of elasticity, *Comput. Methods Appl. Mech. Eng.* 198 (41–44) (2009) 3352–3360.
- [16] S. Hou, Z. Li, L. Wang, W. Wang, A numerical method for solving elasticity equations with interfaces, *Commun. Comput. Phys.* 12 (2) (2012) 595–612.
- [17] S.-H. Chou, D.Y. Kwak, K.T. Wee, Optimal convergence analysis of an immersed interface finite element method, *Adv. Comput. Math.* 33 (2) (2010) 149–168.
- [18] Y. Gong, Z. Li, Immersed interface finite element methods for elasticity interface problems with non-homogeneous jump conditions, *Numer. Math. Theory Methods Appl.* 3 (1) (2010) 23–39.
- [19] X. He, Bilinear immersed finite elements for interface problems, Ph.D. thesis, Virginia Tech, 2009.
- [20] X. He, T. Lin, Y. Lin, Approximation capability of a bilinear immersed finite element space, *Numer. Methods Partial Differ. Equ.* 24 (5) (2008) 1265–1300.
- [21] R. Kafafy, T. Lin, Y. Lin, J. Wang, Three-dimensional immersed finite element methods for electric field simulation in composite materials, *Int. J. Numer. Methods Eng.* 64 (7) (2005) 940–972.
- [22] Z. Li, T. Lin, Y. Lin, R.C. Rogers, An immersed finite element space and its approximation capability, *Numer. Methods Partial Differ. Equ.* 20 (3) (2004) 338–367.
- [23] Z. Li, T. Lin, X. Wu, New Cartesian grid methods for interface problems using the finite element formulation, *Numer. Math.* 96 (1) (2003) 61–98.
- [24] Z. Li, X. Yang, An immersed finite element method for elasticity equations with interfaces, in: *Contemp. Math.*, Amer. Math. Soc., vol. 383, pp. 285–298, 2005.
- [25] T. Lin, X. Zhang, Linear and bilinear immersed finite elements for planar elasticity interface problems, *J. Comput. Appl. Math.* 236 (18) (2012) 4681–4699.
- [26] S. Vallaghé, T. Papadopoulo, A trilinear immersed finite element method for solving the electroencephalography forward problem, *SIAM J. Sci. Comput.* 32 (4) (2010) 2379–2394.
- [27] I. Babuška, M. Suri, On locking and robustness in the finite element method, *SIAM J. Numer. Anal.* 29 (5) (1992) 1261–1293.
- [28] D.N. Arnold, F. Brezzi, J. Douglas Jr., PEERS: a new finite element for plane elasticity, *Jpn. J. Appl. Math.* 1 (2) (1984) 347–367.
- [29] D.N. Arnold, J. Douglas Jr., C.P. Gupta, A family of higher order mixed finite elements for plane elasticity, *Numer. Math.* 45 (1) (1984) 1–22.
- [30] D.N. Arnold, R. Winther, Nonconforming mixed elements for elasticity, *Math. Models Methods Appl. Sci.* 13 (3) (2003) 295–307.
- [31] F. Brezzi, M. Fortin, *Mixed and hybrid finite element methods*, Springer Series in Computational Mathematics, 15, Springer-Verlag, New York, 1991.
- [32] R.S. Falk, Nonconforming finite element methods for the equations of linear elasticity, *Math. Comput.* 57 (196) (1991) 529–550.
- [33] J. Pitkäranta, R. Stenberg, Analysis of some mixed finite element methods for plane elasticity equations, *Math. Comput.* 41 (164) (1983) 399–423.
- [34] R. Stenberg, A family of mixed finite elements for the elasticity problem, *Numer. Math.* 53 (5) (1988) 513–538.
- [35] S.C. Brenner, L.-Y. Sung, Linear finite element methods for planar linear elasticity, *Math. Comput.* 59 (200) (1992) 321–338.
- [36] P. Hansbo, A nonconforming rotated Q_1 approximation on tetrahedra, *Comput. Methods Appl. Mech. Eng.* 200 (9–12) (2011) 1311–1316.
- [37] C.-O. Lee, J. Lee, D. Sheen, A locking-free nonconforming finite element method for planar linear elasticity, *Adv. Comput. Math.* 19 (1–3) (2003) 277–291.
- [38] S. Mao, S. Chen, A quadrilateral nonconforming finite element for linear elasticity problem, *Adv. Comput. Math.* 28 (1) (2008) 81–100.
- [39] Z. Zhang, Analysis of some quadrilateral nonconforming elements for incompressible elasticity, *SIAM J. Numer. Anal.* 34 (2) (1997) 640–663.
- [40] B. Cockburn, D. Schötzau, J. Wang, Discontinuous Galerkin methods for incompressible elastic materials, *Comput. Methods Appl. Mech. Eng.* 195 (25–28) (2006) 3184–3204.
- [41] P. Hansbo, M.G. Larson, Discontinuous Galerkin and the Crouzeix–Raviart element: application to elasticity, *M2AN Math. Model. Numer. Anal.* 37 (1) (2003) 63–72.
- [42] B. Rivière, S. Shaw, M.F. Wheeler, J.R. Whiteman, Discontinuous Galerkin finite element methods for linear elasticity and quasistatic linear viscoelasticity, *Numer. Math.* 95 (2) (2003) 347–376.
- [43] T.P. Wihler, Locking-free adaptive discontinuous Galerkin FEM for linear elasticity problems, *Math. Comput.* 75 (255) (2006) 1087–1102.

- [44] R. Ranacher, S. Turek, Simple nonconforming quadrilateral Stokes element, *Numer. Methods Partial Differ. Equ.* 8 (2) (1992) 97–111.
- [45] M. Bercovier, Perturbation of mixed variational problems, Application to mixed finite element methods, *RAIRO Anal. Numer.* 12 (3) (1978) 211–236.
- [46] C. Johnson, J. Pitkäranta, Analysis of some mixed finite element methods related to reduced integration, *Math. Comput.* 38 (158) (1982) 375–400.
- [47] D. Malkus, T. Hughes, Mixed finite element methods – reduced and selective integration technique: a unification of concepts, *Comput. Methods Appl. Mech. Eng.* 15 (1) (1978) 63–81.
- [48] J.T. Oden, N. Kikuchi, Finite element methods for constrained problems in elasticity, *Int. J. Numer. Methods Eng.* 18 (5) (1982) 701–725.
- [49] Z. Chen, *Finite element methods and their applications*, Springer-Verlag, Berlin, 2005.
- [50] S. Adjerid, T. Lin, A p th degree immersed finite element for boundary value problems with discontinuous coefficients, *Appl. Numer. Math.* 59 (6) (2009) 1303–1321.
- [51] T. Lin, Y. Lin, R. Rogers, M.L. Ryan, A rectangular immersed finite element space for interface problems, *Adv. Comput. Theory Pract.* 7 (2001) 107–114.